Multi-parameter optimization: Development of a morpholin-3-one derivative with an improved kinetic profile for imaging monoacylglycerol lipase in the brain

He, Y.F.; Grether, U.; Taddio, M.F.; Meier, C.; Keller, C.; Edelmann, M.R.; ... ; Gobbi, L.C.

European Journal of Medicinal Chemistry 243 (2022) 114750

Contents lists available at ScienceDirect

European Journal of Medicinal Chemistry

journal homepage: www.elsevier.com/locate/ejmech

Research paper

Multi-parameter optimization: Development of a morpholin-3-one derivative with an improved kinetic profile for imaging monoacylglycerol lipase in the brain

Yingfang He [a], Uwe Grether [b], Marco F. Taddio [a], Carla Meier [a], Claudia Keller [a], Martin R. Edelmann [b,1], Michael Honer [b], Sylwia Huber [b], Matthias B. Wittwer [b], Dominik Heer [b], Hans Richter [b], Ludovic Collin [b], Melanie N. Hug [b,2], Manuel Hilbert [b], Annemarieke G.J. Postmus [d], Anna Floor Stevens [d], Mario van der Stelt [d], Stefanie D. Krämer [a], Roger Schibli [a], Linjing Mu [a,c,*], Luca C. Gobbi [b]

[a] Center for Radiopharmaceutical Sciences, Institute of Pharmaceutical Sciences, Department of Chemistry and Applied Biosciences, ETH Zurich, CH-8093, Zurich, Switzerland
[b] Pharma Research and Early Development, Roche Innovation Center Basel, F. Hoffmann-La Roche Ltd, CH-4070, Basel, Switzerland
[c] Department of Nuclear Medicine, University Hospital Zurich, CH-8091, Zurich, Switzerland
[d] Department of Molecular Physiology, Leiden Institute of Chemistry, Leiden University and Oncode Institute, Leiden, Netherlands

ARTICLE INFO

Keywords:
MAGL
Morpholin-3-one derivatives
PET tracer
Structural optimization
Brain imaging

ABSTRACT

Monoacylglycerol lipase (MAGL) is a gatekeeper in regulating endocannabinoid signaling and has gained substantial attention as a therapeutic target for neurological disorders. We recently discovered a morpholin-3-one derivative as a novel scaffold for imaging MAGL *via* positron emission tomography (PET). However, its slow kinetics *in vivo* hampered the application. In this study, structural optimization was conducted and eleven novel MAGL inhibitors were designed and synthesized. Based on the results from MAGL inhibitory potency, *in vitro* metabolic stability and surface plasmon resonance assays, we identified compound **7** as a potential MAGL PET tracer candidate. [^{11}C]**7** was synthesized *via* direct $^{11}CO_2$ fixation method and successfully mapped MAGL distribution patterns on rodent brains in *in vitro* autoradiography. PET studies in mice using [^{11}C]**7** demonstrated its improved kinetic profile compared to the lead structure. Its high specificity *in vivo* was proved by using MAGL KO mice. Although further studies confirmed that [^{11}C]**7** is a P-glycoprotein (P-gp) substrate in mice, its low P-gp efflux ratio on cells transfected with human protein suggests that it should not be an issue for the clinical translation of [^{11}C]**7** as a novel reversible MAGL PET tracer in human subjects. Overall, [^{11}C]**7** ([^{11}C]RO7284390) showed promising results warranting further clinical evaluation.

1. Introduction

The endocannabinoid system (ECS) is a versatile system that plays an important role in physiological and pathological conditions [1]. It consists of two major G-protein coupled receptors, cannabinoid receptor type-1 and type-2, and endogenous ligands such as 2-arachidonoyl-glycerol (2-AG) and *N*-arachidonoyl ethanolamine, which are referred as endocannabinoids. 2-AG is bio-synthesized 'on-demand' and functions as a retrograde signal to mediate neuronal excitability [2]. Upon the activation of cannabinoid receptor type-1, 2-AG is degraded mainly by monoacylglycerol lipase (MAGL) into fatty acid and glycerol. Pharmacological inhibition in the brain of MAGL, a serine hydrolase comprising 303 amino acid residues, leads to an elevation of 2-AG level in the central nervous system (CNS) and consequently reduces prostaglandin production that results in cytokine-lowering effects [3]. Therefore, MAGL has received tremendous attention as a promising therapeutic

* Corresponding author. Center for Radiopharmaceutical Sciences, Institute of Pharmaceutical Sciences, Department of Chemistry and Applied Biosciences, ETH Zurich, CH-8093, Zurich, Switzerland.
E-mail address: linjing.mu@pharma.ethz.ch (L. Mu).
[1] Present address: Martin R. Edelmann - Department of Pharmacy and Pharmacology, University of Bath, Bath BA2 7AY, UK.
[2] Present address: Melanie N. Hug - Ridgeline discovery, Technologiepark Hochbergerstrasse 60C, CH 4057 Basel, Switzerland.

https://doi.org/10.1016/j.ejmech.2022.114750
Received 1 July 2022; Received in revised form 23 August 2022; Accepted 4 September 2022
Available online 9 September 2022

target against neurological disorders such as Alzheimer's diseases, Parkinson's diseases, multiple sclerosis, amyotrophic lateral sclerosis and traumatic brain injury [4,5].

Positron emission tomography (PET) is a highly sensitive imaging technique that supports drug development and discovery by non-invasive quantification of pharmacological processes *in vivo*. Although a diverse set of MAGL inhibitors with various chemical scaffolds have been patented and published over the last decade [4,11,12], the development of MAGL PET tracers with adequate reversibility *in vivo* is lagging behind [13]. The chemical structures of reversible MAGL PET tracers developed so far are summarized in Fig. 1. Except [^{18}F]T-401 and [^{18}F]YH149 [8,9], the rest of reversible MAGL PET tracers encountered a common issue: a relatively slow brain accumulation within the practical time frame [13]. Among them, [^{11}C]**1** and [^{11}C]**2** were recently developed in our laboratory [10]. Our preliminary results showed that they were recognized by P-glycoprotein (P-gp) in rodents but not in humans. Although [^{11}C]**2** was proved to be MAGL-specific in mice brain, its brain uptake continuously increased during the whole PET scan time period indicating a slow kinetic profile. Similar observation was reported for other MAGL PET probes including [^{11}C]PAD, [^{18}F]MAGL-4-11 and [^{18}F]MAGL2102 (Fig. 1) [6,7]. Such kind of slow kinetics requires longer PET acquisition time to reach the equilibrium for a reliable quantification [14], complicating the measurement of the MAGL-drug interactions in the practical setting.

With the ultimate goal to develop a reversible MAGL PET tracer with rapid brain entry and fast clearance from CNS for clinical translation, we herein report on a structural optimization program based on the chemical structure of compound **2**. The design concept is presented in Fig. 2. The morpholin-3-one scaffold was conserved for non-covalent interactions with binding site residues. Meanwhile, the influences of aromatic substituents and the ether/alkyl linker on the target affinity, metabolic stability and binding kinetics were investigated. From which, we envisioned the development of a novel reversible MAGL PET tracer with more favorable kinetics by accelerating the dissociation from the target site, the elimination from the plasma, and thus from the brain. Aside from the determination of the half-maximal inhibitory concentration (IC_{50}) values of the novel structures, the *in vitro* metabolic stability in liver microsomes or hepatocytes was measured for predicting the *in vivo* clearance in periphery. Moreover, the surface plasmon resonance (SPR) assay was carried out to explore the association rate constants (k_{on}), dissociation rate constants (k_{off}) and dissociation constants (K_d) of the compounds in the target-binding site. The most promising candidate compound **7** with high MAGL inhibitory potency, a medium-to-high clearance and fast dissociation rate constant was selected for further *in vitro* and *in vivo* evaluations. [^{11}C]**7** was synthesized *via* direct $^{11}CO_2$ fixation method. MAGL knockout (KO) and wild-type (WT) mice were enrolled to assess its specificity and kinetic profiles. To investigate the influence of efflux transporters, a triple targeted mutation model (Mdr1a/b-Bcrp KO mice) was further included for *in vivo* evaluations.

2. Results

2.1. Chemistry

Four different procedures were employed to synthesize the desired compounds **3**–**13**. Similar to previously reported synthetic routine for compounds **1** and **2**, compound **3** was prepared via *O*-alkylation of *tert*-butyl 3-hydroxyazetidine-1-carboxylate with benzyl bromide **3a** (Procedure A in Scheme 1). Deprotection of azetidine **3b** by treatment with trifluoroacetic acid at room temperature provided intermediate **3c** which was subsequently reacted with nitro-phenol activated hexahydro-2*H*-pyrido-oxazin-one carboxylate (**15**) to form target compound **3** in 43% yield. Procedure B commences with a Sonogashira coupling of an aryl bromide with *tert*-butyl 3-ethynylazetidine-1-carboxylate to afford *N*-Boc protected intermediates **4b**, **6b**–**8b** and **13b**. After hydrogenation of the triple bond, removal of the Boc group, and subsequent urea formation with activated intermediate **15** in the presence of *N,N*-diisopropylethylamine (DIPEA), morpholine-3-ones **4**, **6**–**8** and **13** were obtained as trifluoroacetate salts with overall yields of 44–56%. As shown in Scheme 2, Procedures C and D began with the formation of phosphonate **5b** and phosphorous ylides **9b**–**12b** followed by a Wittig type reaction yielding *N*-Boc protected *E/Z* double-bond containing azetidines **5c** and **9c-12c**. In analogy to procedure B, the double bond was reduced by hydrogenation catalyzed by palladium on carbon to obtain intermediates **5d** and **9d-12d**. After the deprotection of the *N*-Boc group, the desired products **5** and **9**–**12** were obtained in yields of 14–60% by reacting azetidines **5e**, **9e-12e** with either compound **15** or (4a*R*,8a*S*)-hexahydro-2*H*-pyrido[4,3-b] [1,4]oxazin-3(4*H*)-one (**14**) with triphosgene (BTC). Meanwhile, intermediates **9d-11d** were capable to be synthesized from iodide reagents using procedure B. The corresponding synthetic route and experimental details are provided in supplementary Scheme S1.

2.2. IC_{50} measurement, in vitro metabolism and SPR studies

The results from mouse MAGL IC_{50}, SPR assay and *in vitro* metabolism using mouse liver microsomes and hepatocytes are summarized in Table 1. Compared to the lead compound **2**, compound **3** displayed a higher clearance in liver microsomes and hepatocytes by moving the trifluoromethyl (CF_3) group from 4- to 6-substitution in the aromatic ring. However, this modification also resulted in a dramatic reduction of its MAGL inhibitory activity. In contrast, replacement of the oxygen

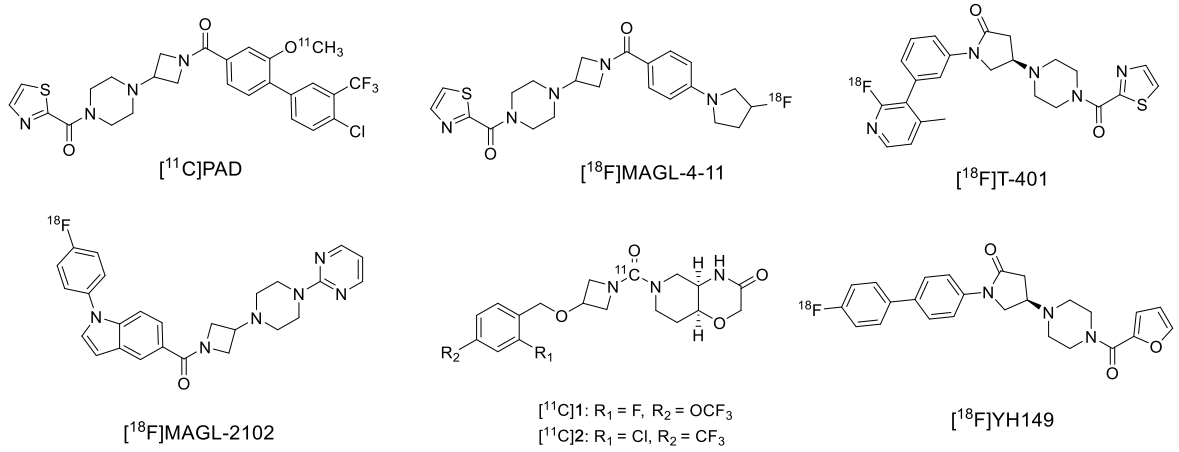

Fig. 1. Chemical structures of reversible MAGL PET ligands [6–10].

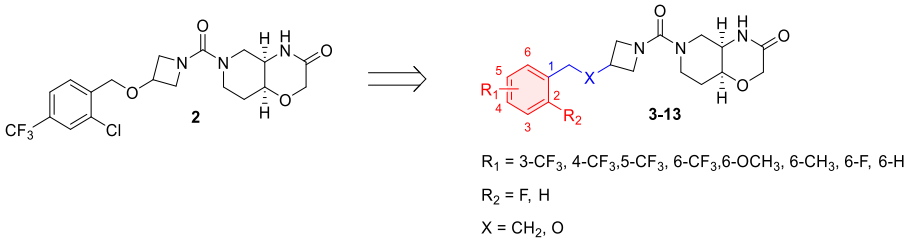

Fig. 2. Chemical modification of compound **2**.

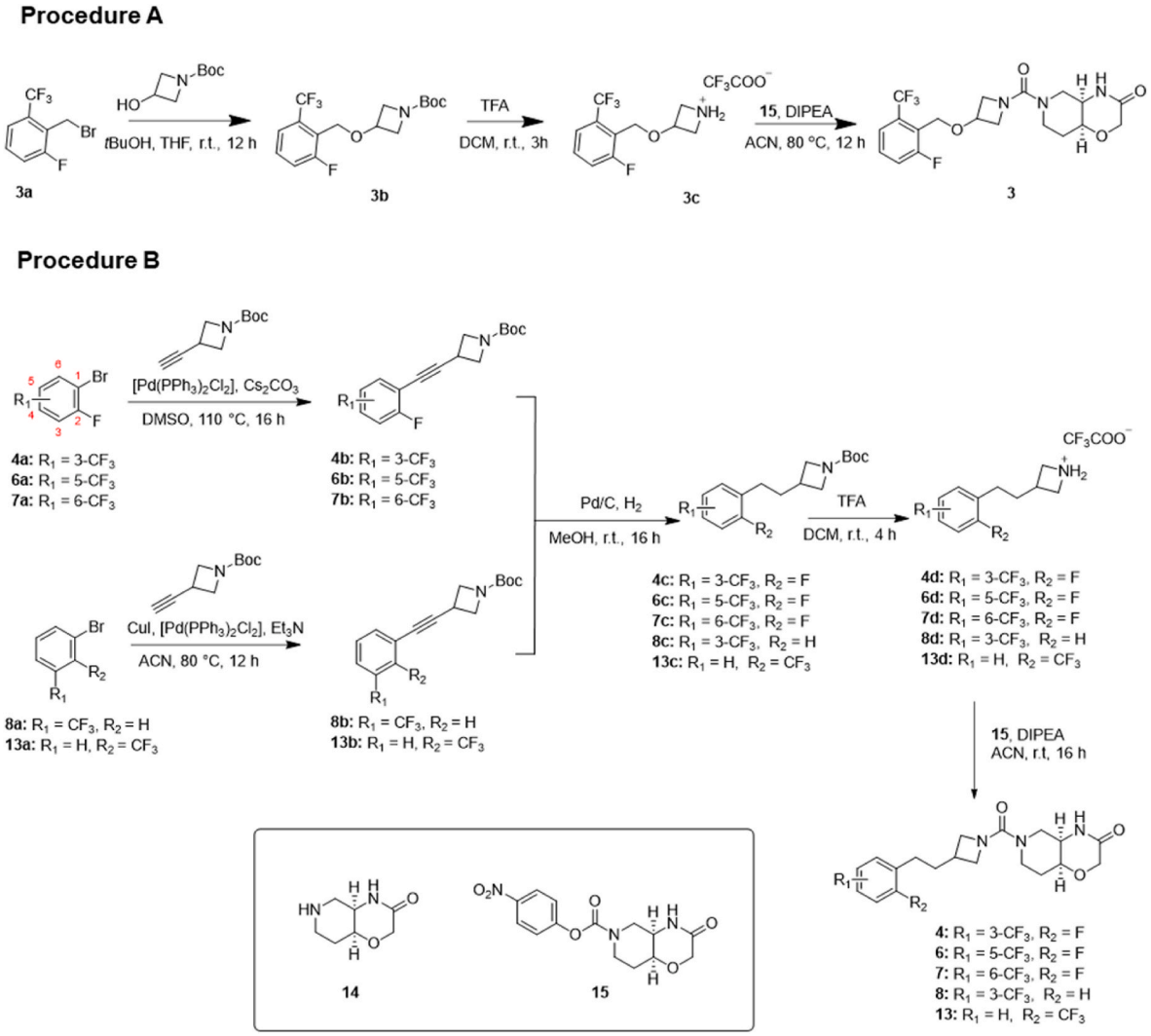

Scheme 1. Chemical syntheses of compounds **3**, **4**, **6**–**8** and **13**.

atom in the side chain with a methylene group profoundly enhanced MAGL inhibitory potency (**5** *vs* **2** and **7** *vs* **3** in Table 1). This may be partially explained by the lipophilic properties of the relevant MAGL binding pocket that is flanked by hydrophobic amino acid residues for matching the aliphatic chain of the natural substrate [14]. Compounds **4**–**7** with CF_3-substituent different positions of the aromatic ring showed comparable MAGL-inhibiting potency, their IC_{50} values ranging from 6.5 nM to 17 nM. Compound **7** with CF_3-substituent at the 6-position of the aromatic ring exhibited the highest clearance (microsome $CL_{int,\ app}$ = 99 μL/min/mg protein, hepatocyte $CL_{int,\ app}$ = 51 μL/min/10^6 cells), while compound **5** containing a 4-CF_3 substituent had much lower clearance (microsome $CL_{int,\ app}$ = 11 μL/min/mg protein, hepatocyte $CL_{int,\ app}$ = 4.9 μL/min/10^6 cells). After identifying the pivotal role of the 6-position in the benzene for clearance, different substituents were used to replace the CF_3 moiety for studying their impact on the binding affinity and metabolic stability. Upon replacing 6-CF_3 to methoxy, methyl, or fluorine (**7** to **9**, **10**, or **11**), a reduction in MAGL inhibitory potency and increased metabolic clearance (except compound **11**) were observed. Mono-substituted aromatic compounds (**8**, **12** and **13**) fell into two-digit nanomolar activities toward MAGL. The binding kinetics of the newly synthesized compounds with low nanomolar activity were further investigated using the SPR assay. The equilibrium dissociation constant (K_d), association rate constant (k_{on}), and dissociation rate constant (k_{off}) of the inhibitor-enzyme complex are shown in Table 1. All the tested

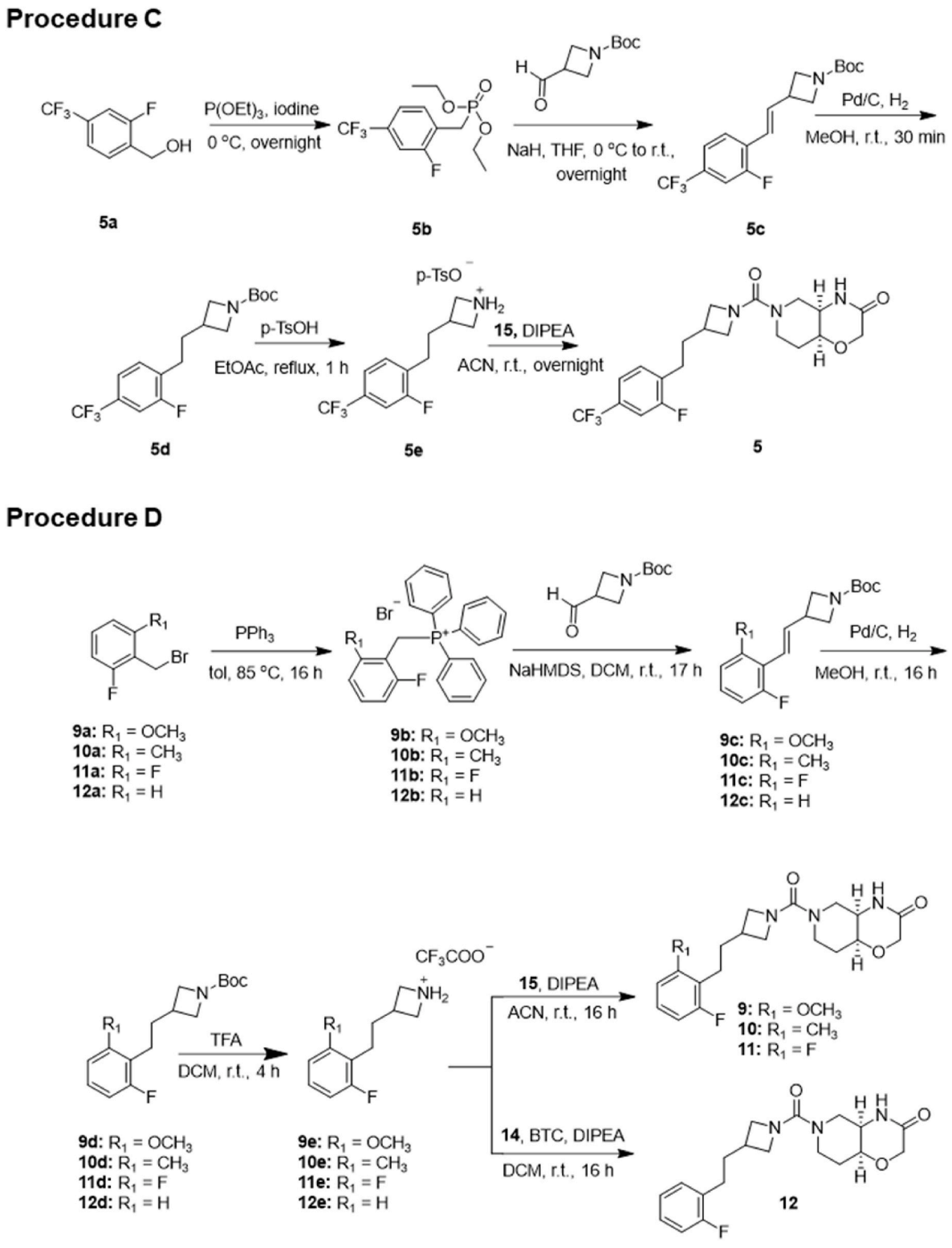

Scheme 2. Chemical syntheses of compounds **5** and **9**–**12**.

compounds bind non-covalently to the immobilized MAGL proteins in the SPR real-time monitoring. The K_d values correlated well with the measured MAGL IC_{50} data. The k_{off} values of compounds **4**, **7**, **10** and **13** were in the range between 0.00558 and 0.00658 s^{-1}. Taken the multiple parameters into consideration, compound **7** with an IC_{50} value of 9.4 ± 3.1 nM (n = 3), a K_d value of 30.0 nM, the highest dissociation rate constant (k_{off} = 0.00658 s^{-1}) and a high metabolic rate as predicted from microsomal and hepatocyte clearance, was selected for advanced profiling prior to radiolabeling.

2.3. Advanced profiling of compound 7

To evaluate the selectivity of compound **7** over the relevant serine hydrolases in the ECS, a gel-based activity-based protein profiling

Table 1
The results of IC_{50} measurements using mouse MAGL protein (n ≥ 3, values are means ± the standard deviation), K_d, k_{on} and k_{off} values measured by SPR (n = 1–2) and *in vitro* metabolism using mouse liver microsomes and hepatocytes (*n.d.* stands for 'not determined').

Compound	IC_{50} (nM)	K_d [b] (nM)	k_{off} (s^{-1})	k_{on} ($M^{-1}s^{-1}$)	Liver microsome Cl_{int} (μL/min/mg protein)	Hepatocyte Cl_{int} (μL/min/10^6 cells)
1 [d]	34 ± 4.8 [a]	24	0.00276	113850	<10 [c]	5.2
2	19 ± 6.5 [a]	5.7	0.00207	364200	<10 [c]	6.8
3	98 ± 40	*n.d.*	*n.d.*	*n.d.*	30	32
4	6.5 ± 1.7	57	0.00588	103600	54	57
5 [d]	6.5 ± 1.6	6.1	0.00204	335200	11	4.9
6	17 ± 4.9	15	0.00392	255800	33	46
7 [d]	9.4 ± 3.1	30	0.00658	214900	99	51
8	19 ± 4.4	29	0.00443	152100	32	25
9	25 ± 6.0	41	0.00234	56570	96	156
10	30 ± 8.0	30	0.00622	208100	133	102
11	481 ± 74	*n.d.*	*n.d.*	*n.d.*	38	36
12	88 ± 25	*n.d.*	*n.d.*	*n.d.*	*n.d.*	45
13	40 ± 4.4	27	0.00558	203500	155	200

[a] Results from Ref. [10].
[b] K_d was calculated from k_{off} divided by k_{on}.
[c] The clearance rate is below the assay sensitivity range.
[d] The SPR was measured in duplicate and the mean value is provided. Corresponding results from individual measurements are presented in supporting information.

(ABPP) assay was applied using mouse brain membrane and cytosol proteomes [15]. Two selective and potent MAGL inhibitors were employed as the positive controls (details in supporting information) [16,17]. As shown in supplementary Figure S1, compound **7** blocked only the fluorescent signals from MAGL under tested conditions. This suggests the high MAGL selectivity of compound **7** over the other hydrolases including fatty acid amide hydrolase (FAAH), diacylglycerol lipase α (DAGL- α) and α/β-hydrolase-domain containing enzymes 6 (ABHD6) and 12 (ABHD12). In P-gp *in vitro* transport experiments, the efflux ratios (ER) of compound **7** in the mouse and human P-gp-transfected cell lines were determined as 5.8 and 1.9, respectively, indicating that the structure could be a P-gp substrate in rodents but not in humans. Moreover, the IC_{50} value of compound **7** towards human MAGL was determined as 3.7 ± 1.2 nM (n = 6), indicating its excellent MAGL potency across species. The free fractions of compound **7** in mouse and human plasma were measured to be 10% and 5%, respectively. These results signify that a low risk of high non-specific binding *in vivo*, according to previously reported literature [18].

2.4. Radiosynthesis of [^{11}C]7

[^{11}C]**7** was synthesized *via* direct [^{11}C]CO_2 fixation using **14** and **7d** as the precursors (Scheme 3). This one-pot, three-step reaction sequence comprises the trapping of [^{11}C]CO_2, the activation *via* a presumable [^{11}C]carbamoyl chloride, and the incorporation of azetidine **7d**. After the semi-preparative high performance liquid chromatography (HPLC) purification, [^{11}C]**7** (1.37 ± 0.25 GBq) was obtained with a molar activity of 59.8 ± 22.9 GBq/μmol at the end of synthesis (n = 20). The radiochemical purity (RCP) was greater than 99%, and the total synthesis time from the end of bombardment was around 30 min.

2.5. In vitro autoradiography

Sagittal brain slices from Wistar rat were utilized to unveil the *in vitro* binding characteristics of [^{11}C]**7**. Representative autoradiograms are presented in Fig. 3. The heterogeneous distribution of [^{11}C]**7** followed the expression pattern of MAGL in the rat brain [19,20]. High

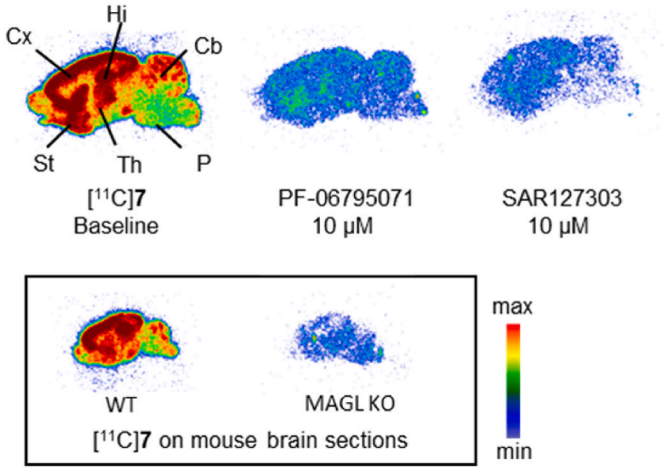

Fig. 3. Representative *in vitro* autoradiograms of [^{11}C]**7** on rat (top) and mouse (bottom) brain sections. Cx, cortex; St, striatum; Hi, hippocampus; Th, thalamus; Cb, cerebellum; P, pons (brainstem).

accumulation was found in the cortex, hippocampus and striatum. Moderate accumulation was detected in the thalamus and cerebellum, followed by low accumulation in the brain stem where a low expression level of MAGL was reported [19,20]. Co-incubation with a MAGL inhibitor, either PF-06795071 or SAR127303 (structures shown in Supplementary Fig. S5), led to a significant reduction of the radioactive signals confirming the *in vitro* specificity of [^{11}C]**7** towards MAGL. Brain sections from MAGL KO and WT mice were further included to evaluate the selectivity of [^{11}C]**7** *in vitro*. A heterogeneous distribution pattern of [^{11}C]**7**, reflecting the target expression patterns, was observed in the WT mouse brain sections. By contrast, low and homogenous signals were seen using brain sections from MAGL KO mouse. These results demonstrate the high specificity and selectivity of [^{11}C]**7** towards MAGL *in vitro*.

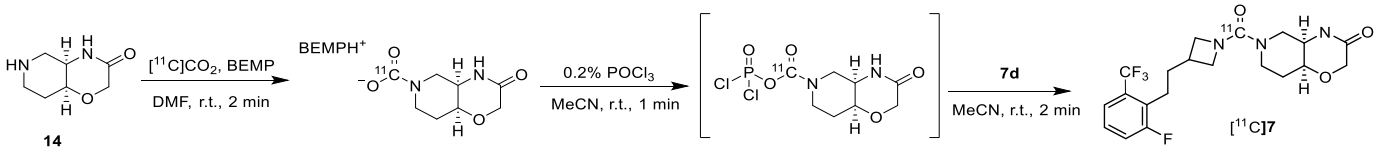

Scheme 3. Radiosynthesis of [^{11}C]**7**.

2.6. Lipophilicity and in vitro stability

The lipophilicity of [^{11}C]**7** was determined as 2.65 ± 0.15 at pH 7.4 using the shake-flask method (n = 3) [21], which falls into the optimal range for brain penetration. The radiochemical purity of [^{11}C]**7** remained above 95% after 40 min incubation at 37 °C in human, rat or mouse serum (Supporting Information, Fig. S4).

2.7. In vivo PET imaging

MAGL KO and WT mice. To investigate the kinetic profile of [^{11}C]**7** *in vivo*, dynamic PET scans were carried out in anaesthetized MAGL KO and WT mice. The time activity curves (TACs) of the whole brain uptake are shown in Fig. 4. The radiotracer exhibited a maximal standardized uptake value (SUV_{max}) of *ca.* 0.4–0.5 in mice brain. Compared to the increasing brain accumulation of [^{11}C]**2** overtime [10], [^{11}C]**7** reached its maximal accumulation in WT mice within 20 min p.i. and slowly washed out afterwards. A strikingly faster clearance was observed in MAGL KO mice brain, confirming the specific and selective binding of the radioligand towards MAGL *in vivo*.

Mdr1a/b-Bcrp KO and WT mice. To investigate the influence from efflux transporters, Mdr1a/b-Bcrp KO mice carrying a disruption of the multi-drug resistance genes and WT mice were enrolled in dynamic PET scans. The whole brain TACs of [^{11}C]**2** and [^{11}C]**7** in Mdr1a/b-Bcrp KO and WT mice are depicted in Fig. 5. Significantly higher brain uptakes were achieved by both radioligands in Mdr1a/b-Bcrp KO mice, confirming that the structures were P-gp substrates in rodents. Compared to [^{11}C]**2**, [^{11}C]**7** exhibited a significantly higher radioactive accumulation and more appropriate kinetic properties in Mdr1a/b-Bcrp KO mice. To understand whether these increased radioactive signals was MAGL-specific, one mouse was pretreated with a potent and selective MAGL inhibitor MAGLi432 [22] (chemical structure shown in Supplementary Fig. S5) before the administration of radiotracer. As illustrated in Fig. 5, a profoundly rapid washout of the radioactivity from the Mdr1a/b-Bcrp KO mouse brain was induced (blue curve), which confirmed the high specificity of [^{11}C]**7** *in vivo*. Fig. 6 shows the axial, sagittal and coronal brain PET images of [^{11}C]**7** in the Mdr1a/b-Bcrp KO and WT mouse. The low brain uptake of [^{11}C]**7** in the WT mouse (Fig. 6A) is in line with its high ER of 5.8 measured *in vitro*. In the Mdr1a/b-Bcrp KO mouse brain, high levels of radioactive signals were revealed for [^{11}C]**7** and its distribution in the different brain regions reflected the MAGL expression pattern in the rodent (Fig. 6B). Blocking with 5 mg/kg MAGLi432, a potent MAGL inhibitor, led to a profound reduction in the level of the radiotracer accumulated in the Mdr1a/b-Bcrp KO mouse brain, as shown in Fig. 6C.

2.8. Radiometabolite analysis

The *in vivo* metabolic stability of [^{11}C]**7** in the mouse brain was further investigated. Fig. 7 shows the radio-UPLC chromatograms from the final formulation and brain homogenates. At 40 min p.i., the intact radiotracer [^{11}C]**7** was the only detectable radioactive peak in the brain extract. We therefore concluded that the radioactive signals in the mouse brain were dominantly presented by the intact structure and the radiometabolites of [^{11}C]**7** showed limited ability to cross the blood-brain barrier.

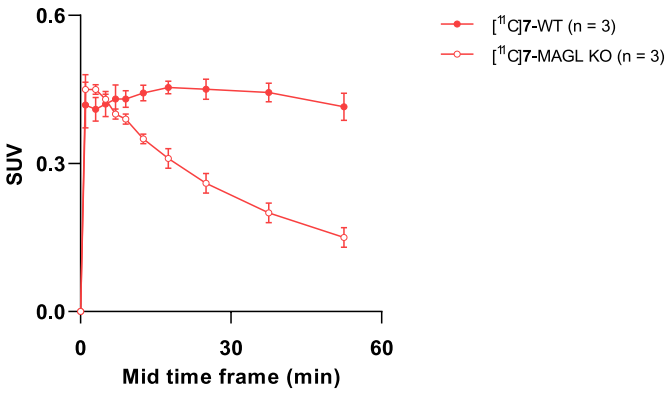

Fig. 4. The whole brain TACs of [^{11}C]**7** in MAGL KO and WT mice.

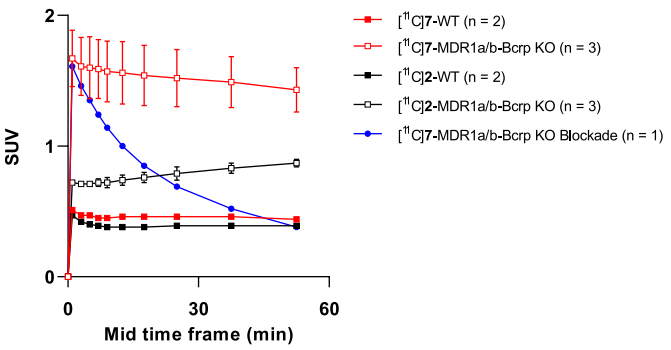

Fig. 5. The whole brain TACs of [^{11}C]**2** and [^{11}C]**7** in Mdr1a/b-Bcrp KO and WT mice.

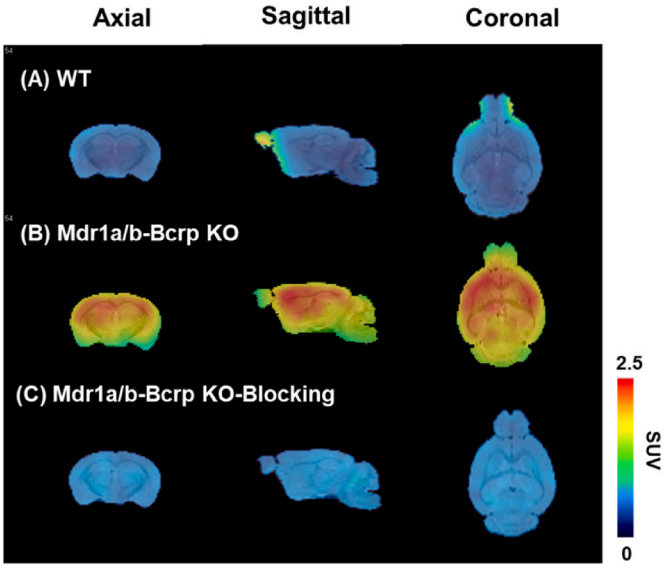

Fig. 6. The axial, sagittal and coronal PET brain images of [^{11}C]**7** in WT mouse (A) and Mdr1a/b-Bcrp KO mouse under baseline (B) and blocking conditions (C) averaged from 13.5 min to 52.5 min p.i.

3. Discussion

In our previous work, we identified [^{11}C]**2** from an industrial morpholin-3-one library (F. Hoffmann-La Roche Ltd) to serve as an entirely novel structure to image MAGL in the CNS [10]. The specificity of [^{11}C]**2** was confirmed *in vivo* using MAGL KO and WT mice. In the meanwhile, the slow kinetic profile of [^{11}C]**2** was disclosed with increasing radioactivity accumulated in mouse brains up to 60 min p.i. This is somehow not surprising as compound **2** was initially designed as a reversible MAGL drug candidate, for which high metabolic stability and a long target residence time are favored for the pursuit of therapeutic efficacy in the treatment. Accordingly, the major objective of the current study was to accelerate the brain clearance of [^{11}C]**2** to consequently improve its kinetic profile as a suitable molecular probe for quantitative PET studies. Eleven compounds were designed and synthesized based on the lead structure **2**. Their IC_{50} values indicated that

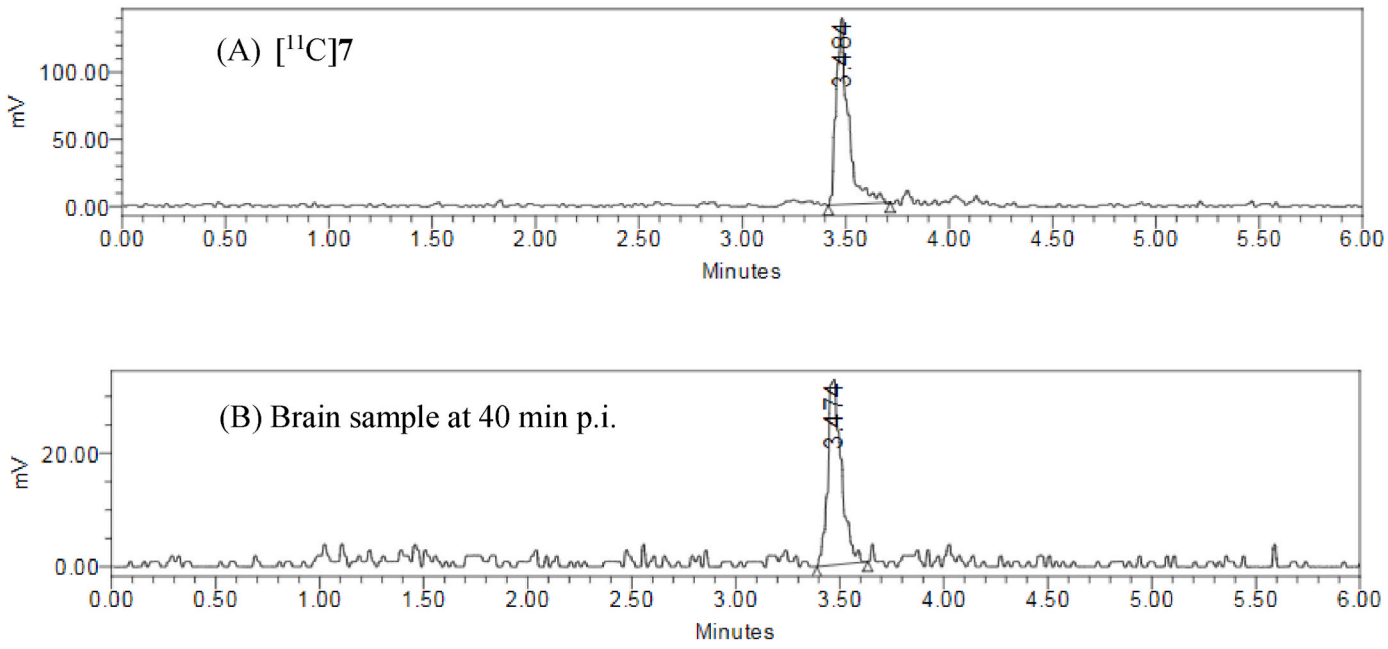

Fig. 7. Radio-UPLC chromatograms of [^{11}C]**7** in the final formulation (A) and the brain homogenate after 40 min p.i. of [^{11}C]**7** (B).

the lipophilic property of the alkyl chain and the position of the trifluoromethyl substituent in the aromatic ring are the essential elements for the regulation of MAGL inhibition potency. Although compounds **4**–**7** displayed high structural similarity and comparable IC_{50} values toward MAGL, compound **7** containing a CF_3-substituent at the position 6 of the benzene ring showed a remarkably high clearance in metabolic stability assays. In addition, compound **7** revealed a faster dissociation rate constant in the MAGL binding pocket compared to those of the other candidates. It was subsequently labeled with carbon-11 for further evaluations.

Remarkably, [^{11}C]**7** reached its peak uptake in the WT mouse brains within a distinctively shorter time period than [^{11}C]**2** (17.5 min p.i. for [^{11}C]**7** *vs.* 52.5 min p.i. for [^{11}C]**2** [10]). This could be attributed to the faster metabolism of [^{11}C]**7** in periphery in addition to its increased dissociation from MAGL protein as determined in the SPR assay (Table 1). However, it is hard to speculate the major contributor based on the current results because the interactions between tracer and target macromolecules *in vivo* are more complex than in *in vitro* assays running under closed system conditions. Further PET kinetic studies with mathematical modelling are required to elucidate the key determinant behind this improved kinetic profile. The *in vivo* specificity of [^{11}C]**7** in the mouse brain was confirmed by 63% reduction of the radioactive signals in the MAGL KO mice compared to the WT mice. To investigate the impact of efflux transporters on mice brain uptake, PET studies were then conducted with triplet-mutated mice carrying a disruption of efflux transporters. As expected, higher brain uptakes were accomplished by [^{11}C]**2** and [^{11}C]**7** in Mdr1a/b-Bcrp KO mice brain. Of note, [^{11}C]**7** achieved a significantly higher brain penetration in Mdr1a/b-Bcrp KO mice than that of [^{11}C]**2** ([^{11}C]**7**: 1.67 SUV at 2 min p.i. *vs.* [^{11}C]**2**: 0.72 SUV at 2 min p.i.). This improvement might be owing to the reduced molecular weight, slightly increased lipophilicity and decreased topological surface area (TPSA) of [^{11}C]**7** (M_w = 429.17, log$D_{7.4}$ = 2.65, TPSA = 61.88 using ChemDraw 19.0) compared to [^{11}C]**2** (M_w = 447.12, log$D_{7.4}$ = 2.21 [10], TPSA = 71.11 using ChemDraw 19.0). Taken together with the low ER value of 1.9 obtained from porcine kidney epithelial cells overexpressing human P-gp, [^{11}C]**7** is not expected as a substrate for efflux transporters in human subjects, and therefore holds a great potential to achieve a high brain uptake in further clinical translation. So far, it remains unclear whether [^{11}C]**7** would have a slower brain washout in higher species and whether the volume of distribution could be stable and measurable within the practicable imaging time of carbon-11. In this perspective, a fluorine-18 labeled version of compound **7** without structural modification or the methyl-substituted analog compound **10** that has higher metabolic clearance capacity could offer a solution.

4. Conclusion

In conclusion, [^{11}C]**7** is a promising reversible MAGL probe that could serve as a potential clinical candidate with an entirely novel chemical scaffold for imaging MAGL in the brain. It demonstrated high specificity, selectivity and reversible target binding towards MAGL *in vivo*, as well as the absence of confounding radiometabolites in the mouse brain. In the structural optimization process, the results of metabolic stability and surface plasmon resonance provided valuable guidance in the compound selection prior to the radiolabeling, and ultimately led to the identification of [^{11}C]**7** with improved kinetic profile *in vivo*. This finding may provide useful hints for the structural optimization of PET probes that encountered slow pharmacokinetics for neuroimaging.

5. Experimental section

General Information. All chemicals, reagents and solvents for the synthesis and analysis of compounds were purchased from commercial sources and used without further purification. The key intermediate, (4a*R*,8a*S*)-hexahydro-2*H*-pyrido[4,3-b][1,4]oxazin-3(4*H*)-one (**14**), was prepared from its racemic commercial source (ChemBridge Corporation) and purified by preparative chiral HPLC (ReprosilChiral NR column) using an isocratic mixture of EtOH (containing 0.05% of NH_4OAc): *n*-heptane (30:70). The 4-nitrophenyl (4a*R*,8a*S*)-3-oxohexahydro-2*H*-pyrido[4,3-b][1,4]oxazine-6(5*H*)-carboxylate (**15**) was prepared according to the previously described method [10]. All the reactions were monitored by thin-layer chromatography (TLC) performed on Merck TLC glass sheets (silica gel 60 F254) or a Waters Acquity ultra-performance liquid chromatography (UPLC) equipped with a single quadrupole mass spectrometer (MS). Fast column chromatography was carried out using silica gel (Sigma-Aldrich, mesh size 230–400). Nuclear magnetic resonance spectra were acquired on Bruker Avance FT-NMR spectrometer 300, 400 or 600 MHz instruments. Chemical shifts (δ) are reported in parts per

million (ppm), relative to the residual solvent peak or tetramethylsilane (TMS). High resolution mass spectra were recorded by an Agilent liquid chromatography (LC) system consisting of Agilent 1290 high pressure gradient system, a CTC PAL auto sampler and an Agilent 6520 quadrupole time-of-flight MS. The separation in Agilent LC-system was achieved by Zorbax Eclipse Plus C18 column at 55 °C (2.1 × 50 mm, 1.8 μm; mobile phase A = 0.02% formic acid in water, mobile phase B = acetonitrile with 0.01% formic acid at flow 0.8 mL/min; gradient: 0 min 5%B, 0.3 min 5% B, 4.5 min 99%B, 5 min 99%B). The injection volume was 2 μL, and the ionization was performed in Agilent multimode source. The system was run in "2 GHz extended dynamic range" mode, resulting in a resolution of about 10 000 at m/z = 922. Mass accuracy was ensured by internal drift correction. Purity of all biologically tested compounds was determined by LC-MS, and greater than 95%.

5.1. Chemistry

Procedure A. *tert*-Butyl 3-((2-fluoro-6-(trifluoromethyl)benzyl)oxy) azetidine-1-carboxylate (**3b**). To a solution of *tert*-butyl 3-hydroxyazetidine-1-carboxylate (674 mg, 3.89 mmol) in anhydrous THF (5 mL), potassium *tert*-butoxide (1.0 M solution in THF, 5.84 mL, 5.84 mmol) and **3a** (1.00 g, 3.89 mmol) were added. After stirring at room temperature for 12 h, the mixture was poured into water (10 mL) and extracted three times with ethyl acetate (20 mL × 3). The combined organic layers were dried over anhydrous Na_2SO_4 and filtered. The filtrate was concentrated under reduced pressure, purified by flash chromatography (SiO_2, petroleum ether: ethyl acetate = 10/1 to 2/8) to obtain the desired product as a colorless oil (1100 mg, 81%). LC-MS (ESI): *m/z* = 294.0 $[M\text{-}t\text{Bu} + H]^+$.

3-((2-Fluoro-6-(trifluoromethyl)benzyl)oxy)azetidine 2,2,2-trifluoroacetate (**3c**). To a solution of **3b** (400 mg, 1.15 mmol) in DCM (5 mL) was added TFA (2.00 mL). The reaction mixture was stirred at room temperature for 12 h. The reaction mixture was concentrated under reduced pressure and dried to afford crude product (300 mg) as a yellow oil, which was used in the next step without any further purification. LC-MS (ESI): *m/z* = 250.0 $[M+H]^+$.

(4a*R*,8a*S*)-6-(3-((2-Fluoro-6-(trifluoromethyl)benzyl)oxy)azetidine-1-carbonyl)hexahydro-2*H*-pyrido[4,3-b][1,4] oxazin-3(4*H*)-one (**3**). To a solution of **15** (106 mg, 0.33 mmol) in MeCN (10 mL) was added DIPEA (107 mg, 0.83 mmol) and **3c** (100 mg, 0.28 mmol). The reaction mixture was stirred at 80 °C for 12 h. The solvent was removed under reduced pressure and the crude residue was purified by reversed-phase HPLC to yield the desired product as a white solid (53 mg, 43%). ^{1}H NMR (600 MHz, Chloroform-*d*) δ 7.54–7.48 (m, 1H), 7.48–7.43 (m, 1H), 7.31 (t, *J* = 8.8 Hz, 1H), 6.18 (br d, *J* = 3.6 Hz, 1H, -NHCO-), 4.62 (s, 2H), 4.37 (tt, *J* = 6.6, 4.4 Hz, 1H), 4.32–4.26 (m, 1H), 4.23–4.15 (m, 2H), 4.12 (dd, *J* = 8.9, 7.0 Hz, 1H), 3.96 (d, *J* = 2.8 Hz, 1H), 3.93 (ddd, *J* = 9.2, 4.4, 0.8 Hz, 1H), 3.89–3.83 (m, 2H), 3.55–3.45 (m, 1H), 3.42–3.34 (m, 1H), 3.13–3.00 (m, 2H), 1.91 (dd, *J* = 14.4, 2.7 Hz, 1H), 1.85–1.74 (m, 1H). ^{13}C NMR (151 MHz, Chloroform-*d*) δ 168.22, 162.25 (d, J_{C-F} = 250.2 Hz), 162.09, 131.41 (d, J_{C-F} = 34.6 Hz), 130.49 (d, J_{C-F} = 9.2 Hz), 123.43 (q, J_{C-F} = 274.1 Hz), 122.79 (d, J_{C-F} = 16.9 Hz), 122.02, 119.56 (d, J_{C-F} = 23.0 Hz), 69.47, 68.38, 67.68, 60.49, 58.44, 58.25, 49.57, 46.20, 39.77, 29.55. HRMS (ESI) calculated for $[M+H]^+$/$C_{19}H_{22}F_4N_3O_3^+$: 432.1541 m/z, found: 432.1546 m/z.

Procedure B. *tert*-Butyl 3-((2-fluoro-3-(trifluoromethyl)phenyl) ethynyl)azetidine-1-carboxylate (**4b**). To a solution of **4a** (405 mg, 1.67 mmol) and *tert*-butyl 3-ethynylazetidine-1-carboxylate (300 mg, 1.66 mmol) in DMSO (10 mL) were added $Pd(PPh_3)_2Cl_2$ (117 mg, 0.17 mmol) and cesium carbonate (1.08 g, 3.31 mmol) at 25 °C. The mixture was stirred at 110 °C for 16 h under N_2 protection, poured into brine (30 mL) and extracted with ethyl acetate (30 mL × 2). The organic layers were washed with water (20 mL × 2). The organic layers were dried over Na_2SO_4, filtered and concentrated *in vacuo* to give a residue, which was purified by column chromatography (SiO_2, petroleum ether: ethyl acetate = 10:1 to 3:1) to give the desired product as a colorless oil (139 mg, 22%). ^{1}H NMR (400 MHz, Methanol-d_4) δ 7.78–7.72 (m, 1H), 7.70–7.63 (m, 1H), 7.38–7.30 (m, 1H), 4.27 (t, *J* = 8.5 Hz, 2H), 4.03–3.92 (m, 2H), 3.80–3.63 (m, 1H), 1.46 (s, 9H). LC-MS (ESI): *m/z* = 288.0 $[M\text{-}t\text{Bu} + H]^+$.

tert-Butyl 3-((2-fluoro-3-(trifluoromethyl)phenyl)ethynyl)azetidine-1-carboxylate (**4c**). To a mixture of **4b** (130 mg, 0.38 mmol) in methanol (5 mL) was added 10% Pd/C (50.0 mg, 0.05 mmol) and the mixture was stirred at 25 °C under H_2 (15 psi) for 16 h. The mixture was filtered and the filtrate was concentrated *in vacuo* to give a residue, which was purified by column chromatography (SiO_2, petroleum ether: ethyl acetate = 15:1 to 5:1) to the desired product as a colorless oil (88 mg, 57%). ^{1}H NMR (400 MHz, Chloroform-*d*) δ 7.49–7.43 (m, 1H), 7.39–7.33 (m, 1H), 7.19–7.13 (m, 1H), 4.00 (t, *J* = 8.3 Hz, 2H), 3.55 (dd, *J* = 8.3, 5.5 Hz, 2H), 2.72–2.58 (m, 2H), 2.56–2.39 (m, 1H), 1.91 (q, *J* = 7.7 Hz, 2H), 1.43 (s, 9H). LC-MS (ESI): *m/z* = 292.0 $[M\text{-}t\text{Bu} + H]^+$.

3-(2-Fluoro-3-(trifluoromethyl)phenethyl)azetidine 2,2,2-trifluoroacetate (**4d**). To a solution of **4c** (80.0 mg, 0.23 mmol) in DCM (2 mL) was added trifluoroacetic acid (0.20 mL, 2.60 mmol) and the mixture was stirred at 25 °C for 4 h. The reaction solution was concentrated under reduced pressure to give a crude product, which was directly used in the next step without any further purification. LC-MS (ESI): *m/z* = 248.4 $[M+H]^+$.

(4a*R*,8a*S*)-6-(3-(2-Fluoro-3-(trifluoromethyl)phenethyl)azetidine-1-carbonyl)hexahydro-2*H*-pyrido[4,3-b][1,4] oxazin-3(4*H*)-one (**4**). To solution of **4d** (40.0 mg, 0.11 mmol) and DIPEA (0.11 mL, 0.65 mmol) in MeCN (2 mL) was added **15** (36.0 mg, 0.11 mmol). Then the mixture was stirred at 25 °C for 16 h. The solution was concentrated *in vacuo* to give a residue, which was purified by preparative HPLC (column: Phenomenex Luna C18 75 × 30 mm, 3 μm, mobile phase: A/B = 0.1%TFA in water/acetonitrile, condition: 25 mL/min, A/B from 58/42 to 28/72) and then lyophilized to give the desired product as a colorless oil (25 mg, 53%). ^{1}H NMR (600 MHz, Chloroform-*d*) δ 7.48–7.45 (m, 1H), 7.39–7.34 (m, 1H), 7.16 (t, *J* = 7.7 Hz, 1H), 6.30 (br d, *J* = 3.0 Hz, 1H, -NHCO-), 4.32–4.28 (m, 1H), 4.21–4.17 (m, 1H), 4.09 (t, *J* = 8.3 Hz, 1H), 4.02 (t, *J* = 8.3 Hz, 1H), 3.96 (s, 1H), 3.88 (dd, *J* = 13.0, 4.9 Hz, 1H), 3.65 (dd, *J* = 8.3, 5.9 Hz, 1H), 3.59 (dd, *J* = 8.2, 5.9 Hz, 1H), 3.49–3.45 (m, 1H), 3.42–3.37 (m, 1H), 3.14–2.99 (m, 2H), 2.66 (t, *J* = 7.6 Hz, 2H), 2.60–2.55 (m, 1H), 1.95–1.90 (m, 3H), 1.81–1.75 (m, 1H). ^{13}C NMR (151 MHz, Chloroform-*d*) δ 168.37, 162.29, 157.99 (d, J_{C-F} = 254.6 Hz), 134.47 (d, J_{C-F} = 5.4 Hz), 129.85 (d, J_{C-F} = 15.4 Hz), 125.16 (q, J_{C-F} = 4.3 Hz), 123.95 (d, J_{C-F} = 4.4 Hz), 122.71 (q, J_{C-F} = 272.3 Hz), 118.50, 69.48, 67.66, 56.57, 49.58, 46.17, 39.74, 34.72, 29.59, 28.94, 26.31. HRMS (ESI) calculated for $[M+H]^+$/$C_{20}H_{24}F_4N_3O_3^+$: 430.1748 m/z, found: 430.1750 m/z.

tert-Butyl 3-((2-fluoro-5-(trifluoromethyl)phenyl)ethynyl)azetidine-1-carboxylate (**6b**). The procedure described for the synthesis of **4b** was applied to **6a** (675 mg, 2.78 mmol), *tert*-butyl 3-ethynylazetidine-1-carboxylate (500 mg, 2.76 mmol), $Pd(PPh_3)_2Cl_2$ (195 mg, 0.28 mmol) and cesium carbonate (1.80 g, 5.52 mmol) in 10 mL DMSO to give the desired product as a colorless oil (214 mg, 20%). ^{1}H NMR (400 MHz, Chloroform-*d*) δ 7.73–7.67 (m, 1H), 7.59–7.52 (m, 1H), 7.18 (t, *J* = 8.7 Hz, 1H), 4.23 (t, *J* = 8.5 Hz, 2H), 4.05 (dd, *J* = 8.2, 6.4 Hz, 2H), 3.66–3.53 (m, 1H), 1.45 (s, 9H). LC-MS (ESI): *m/z* = 288.1 $[M\text{-}t\text{Bu} + H]^+$.

tert-Butyl 3-(2-fluoro-5-(trifluoromethyl)phenethyl)azetidine-1-carboxylate (**6c**). The procedure described for the synthesis of **4c** was applied to **6b** (205 mg, 0.60 mmol) and 10% Pd/C (50.0 mg, 0.05 mmol) in methanol (5 mL) to give the desired product as a grey solid (128 mg, 56%). ^{1}H NMR (400 MHz, DMSO-d_6) δ 7.85–7.73 (m, 1H), 7.69–7.61 (m, 1H), 7.39 (t, *J* = 9.2 Hz, 1H), 3.88 (s, 2H), 3.47 (s, 2H), 2.64 (t, *J* = 7.7 Hz, 2H), 2.48–2.37 (m, 1H), 1.83 (q, *J* = 7.7 Hz, 2H), 1.37 (s, 9H). LC-MS (ESI): *m/z* = 292.3 $[M\text{-}t\text{Bu} + H]^+$.

3-(2-Fluoro-5-(trifluoromethyl)phenethyl)azetidine 2,2,2-trifluoroacetate (**6d**). The procedure described for the synthesis of **4d** was applied to **6c** (120 mg, 0.35 mmol) and trifluoroacetic acid (0.30 mL, 3.89 mmol) to a crude product, which was directly applied to next step

without any further purification. LC-MS (ESI): m/z = 248.4 $[M+H]^+$.

(4a*R*,8a*S*)-6-(3-(2-Fluoro-5-(trifluoromethyl)phenethyl)azetidine-1-carbonyl)hexahydro-2*H*-pyrido[4,3-b][1,4]oxazin-3(4*H*)-one (**6**). The procedure described for the synthesis of **4** was applied to **6d** (40.0 mg, 0.11 mmol), DIPEA (0.11 mL, 0.65 mmol), **15** (36.0 mg, 0.11 mmol) in MeCN (2 mL). The crude was purified by preparative HPLC (column: Phenomenex Synergi C18 150 × 25 mm, 10 μm, mobile phase: A/B = 0.1%TFA in water/acetonitrile, condition: 25 mL/min, A/B from 59/41 to 29/71) and then lyophilized to give the desired product as a colorless oil (21 mg, 44%). ^{1}H NMR (400 MHz, DMSO-d_6) δ 8.13 (d, J = 3.9 Hz, 1H, -NHCO-), 7.76 (d, J = 6.7 Hz, 1H), 7.69–7.63 (m, 1H), 7.40 (t, J = 9.0 Hz, 1H), 4.10–4.00 (m, 2H), 3.99–3.88 (m, 4H), 3.71 (dd, J = 4.5, 12.4 Hz, 1H), 3.60–3.52 (m, 2H), 3.48 (d, J = 13.7 Hz, 1H), 3.23–3.16 (m, 1H), 2.87–2.74 (m, 2H), 2.68–2.62 (m, 2H), 1.83 (q, J = 7.7 Hz, 2H), 1.78–1.66 (m, 2H). ^{13}C NMR (151 MHz, Chloroform-*d*) δ 168.55, 162.82 (d, J_{C-F} = 250.5 Hz), 162.26, 129.17 (d, J_{C-F} = 17.5 Hz), 127.85, 126.44, 125.39, 123.77 (q, J_{C-F} = 271.9 Hz), 115.90 (d, J_{C-F} = 23.8 Hz), 69.45, 67.59, 56.57, 49.55, 46.13, 39.72, 34.62, 29.56, 28.93, 26.48. HRMS (ESI) calculated for $[M+H]^+/C_{20}H_{24}F_4N_3O_3^+$: 430.1748 m/z, found: 430.1753 m/z.

tert-Butyl 3-((2-fluoro-6-(trifluoromethyl)phenyl)ethynyl)azetidine-1-carboxylate (**7b**). The procedure described for the synthesis of **4b** was applied to **7a** (270 mg, 1.11 mmol), *tert*-butyl 3-ethynylazetidine-1-carboxylate (200 mg, 1.10 mmol), $Pd(PPh_3)_2Cl_2$ (78.0 mg, 0.11 mmol) and cesium carbonate (719 mg, 2.21 mmol) in DMSO (5 mL) to give the desired product as a colorless oil (127 mg, 32%). ^{1}H NMR (400 MHz, DMSO-d_6) δ 7.77–7.57 (m, 3H), 4.22 (t, J = 7.9 Hz, 2H), 3.90–3.68 (m, 3H), 1.39 (s, 9H). LC-MS (ESI): m/z = 287.9 [M-*t*Bu + H]$^+$.

tert-Butyl 3-(2-fluoro-6-(trifluoromethyl)phenethyl)azetidine-1-carboxylate (**7c**). The procedure described for the synthesis of **4c** was applied to **7b** (110 mg, 0.32 mmol) and 10% Pd/C (50.0 mg, 0.05 mmol) in methanol (5 mL) to give the desired product as a yellow oil (95 mg, 68%). ^{1}H NMR (400 MHz, DMSO-d_6) δ 7.68–7.41 (m, 3H), 3.91 (s, 2H), 3.48–3.41 (m, 2H, overlapped with water residue), 2.73–2.60 (m, 2H), 2.57–2.52 (m, 1H, overlapped with solvent peak), 1.90–1.68 (m, 2H), 1.35 (s, 9H). LC-MS (ESI): m/z = 292.0 [M-*t*Bu + H]$^+$.

3-(2-Fluoro-6-(trifluoromethyl)phenethyl)azetidine (**7d**). The procedure described for the synthesis of **4d** was applied to **7c** (80.0 mg, 0.23 mmol) and trifluoroacetic acid (0.20 mL, 2.60 mmol) to give a crude product which was directly applied to next step without any further purification. LC-MS (ESI): m/z = 248.0 $[M+H]^+$. Regarding the precursor for radiolabeling, *p*-toluenesulfonic acid was employed as the acid for deprotection. To a solution of **7c** (800 mg, 2.3 mmol) in ethyl acetate (5 ml) was added 4-methylbenzenesulfonic acid monohydrate (438 mg, 2.3 mmol). The mixture was heated at reflux for 1 h, cooled down to room temperature, and kept at 4 °C overnight. The suspension was filtered, washed with Et_2O, resolved in ethyl acetate, and treated with pentane/Et_2O for recrystallization. ^{1}H NMR (600 MHz, DMSO-d_6) δ 8.63–8.31 (m, 2H), 7.57 (ddd, J = 9.6, 8.0, 1.0 Hz, 1H), 7.59 (dd, J = 7.9, 1.0 Hz, 1H), 7.52 (td, J = 8.1, 5.8 Hz, 1H), 7.47 (d, J = 8.1 Hz, 2H), 7.11 (dd, J = 8.5, 0.6 Hz, 2H), 4.06–3.97 (m, 2H), 3.64–3.57 (m, 2H), 2.87–2.76 (m, 1H), 2.69–2.63 (m, 2H), 2.28 (s, 3H), 1.88–1.80 (m, 2H). HRMS (ESI) calculated for $[M+H]^+/C_{12}H_{14}F_4N^+$: 248.1057 m/z, found: 248.1062 m/z.

(4a*R*,8a*S*)-6-(3-(2-Fluoro-6-(trifluoromethyl)phenethyl)azetidine-1-carbonyl)hexahydro-2*H*-pyrido[4,3-b][1,4]oxazin-3(4*H*)-one (**7**). The procedure described for the synthesis of **4** was applied to **7d** (30.0 mg, 0.08 mmol), DIPEA (0.08 mL, 0.49 mmol), **15** (27.0 mg, 0.08 mmol) in MeCN (2 mL). The crude was purified by preparative HPLC (column: phenomenex Luna C18 150 × 25 mm, 10 μm, mobile phase: A/B = 0.225% formic acid in water/acetonitrile, condition: 25 mL/min, A/B from 62/38 to 32/68) and then lyophilized to give the desired product as a yellow gum (20 mg, 56%). ^{1}H NMR (600 MHz, Chloroform-*d*) δ 7.44 (d, J = 7.9 Hz, 1H), 7.30 (td, J = 7.7, 5.8 Hz, 1H), 7.25–7.19 (m, 1H), 6.22 (br s, 1H, -NHCO-), 4.32–4.26 (m, 1H), 4.22–4.17 (m, 1H), 4.11 (t, J = 8.3 Hz, 1H), 4.06 (t, J = 8.3 Hz, 1H), 3.97 (br d, J = 2.6 Hz, 1H), 3.89 (br dd, J = 13.1, 4.6 Hz, 1H), 3.67 (dd, J = 8.2, 5.9 Hz, 1H), 3.62 (dd, J = 8.2, 5.8 Hz, 1H), 3.53–3.45 (m, 1H), 3.43–3.37 (m, 1H), 3.12–3.00 (m, 2H), 2.77–2.68 (m, 2H), 2.67–2.58 (m, 1H), 1.92 (br d, J = 6.3 Hz, 1H), 1.99–1.86 (m, 2H), 1.84–1.74 (m, 1H). ^{13}C NMR (151 MHz, Chloroform-*d*) δ 168.29, 162.28, 161.69 (d, J_{C-F} = 246.1 Hz), 130.42 (q, J_{C-F} = 30.1 Hz), 127.91, 127.73, 123.89 (q, J_{C-F} = 273.6 Hz), 121.83, 119.00 (d, J_{C-F} = 23.3 Hz), 69.50, 67.67, 56.58, 56.52, 49.61, 46.18, 39.70, 34.88, 29.59, 23.47. HRMS (ESI) calculated for $[M+H]^+/C_{20}H_{24}F_4N_3O_3^+$: 430.1748 m/z, found: 430.1751 m/z.

tert-Butyl 3-((3-(trifluoromethyl)phenyl)ethynyl)azetidine-1-carboxylate (**8b**). To a mixture of **8a** (200 mg, 1.10 mmol) and 3-iodobenzotrifluoride (302 mg, 1.11 mmol) in MeCN (2 mL) was added copper (I) iodide (22.9 mg, 0.12 mmol), $Pd(PPh_3)_2Cl_2$ (150 mg, 0.21 mmol) and triethylamine (0.40 mL, 2.87 mmol) at 25 °C. The mixture was stirred at 80 °C for 12 h under N_2. The mixture was added brine (30 mL) and extracted with ethyl acetate (30 mL × 1). The organic layer was dried over Na_2SO_4, filtered and concentrated *in vacuo*. The residue was purified by flash column (SiO_2, petroleum ether: ethyl acetate = 20:1 to 5:1) to give the desired product as a colorless oil (77 mg, 18%). ^{1}H NMR (400 MHz, Methanol-d_4) δ 7.76–7.64 (m, 3H), 7.61–7.52 (m, 1H), 4.34–4.20 (m, 2H), 4.09–3.95 (m, 2H), 3.81–3.58 (m, 1H), 1.47 (s, 9H). LC-MS (ESI): m/z = 269.9 [M-*t*Bu + H]$^+$.

tert-Butyl 3-(3-(trifluoromethyl)phenethyl)azetidine-1-carboxylate (**8c**). The procedure described for the synthesis of **4c** was applied to **8b** (72.0 mg, 0.22 mmol) and 10% Pd/C (30.0 mg, 0.03 mmol) in methanol (2 mL) to give the desired product as a colorless oil (55 mg, 70%). ^{1}H NMR (400 MHz, Methanol-d_4) δ 7.61–7.40 (m, 4H), 4.09–3.82 (m, 2H), 3.67–3.47 (m, 2H), 2.82–2.64 (m, 2H), 2.62–2.48 (m, 1H), 1.95 (q, J = 7.7 Hz, 2H), 1.44 (s, 9H). LC-MS (ESI): m/z = 274.3 [M-*t*Bu + H]$^+$.

3-(3-(Trifluoromethyl)phenethyl)azetidine 2,2,2-trifluoroacetate (**8d**). The procedure described for the synthesis of **4d** was applied to **8c** (50.0 mg, 0.15 mmol) and trifluoroacetic acid (0.08 mL, 1.08 mmol) in 1 mL DCM to obtain a crude product, which was directly applied in the next step without any further purification. LC-MS (ESI): m/z = 230.0 $[M+H]^+$.

(4a*R*,8a*S*)-6-(3-(3-(Trifluoromethyl)phenethyl)azetidine-1-carbonyl)hexahydro-2*H*-pyrido[4,3-b][1,4]oxazin-3(4*H*)-one (**8**). The procedure described for the synthesis of **4** was applied to **15** (46.8 mg, 0.15 mmol), **8d** (50.0 mg, 0.15 mmol) and DIPEA (0.15 mL, 0.85 mmol) in MeCN (2 mL). The crude was purified by preparative HPLC (column: Phenomenex Synergi C18 150 × 25 mm, 10 μm, mobile phase: A/B = 0.1%TFA in water/acetonitrile, condition: 27 mL/min, A/B from 63/37 to 23/67) and then lyophilized to give the desired product as a colorless oil (28 mg, 47%). ^{1}H NMR (400 MHz, DMSO-d_6) δ 8.14 (d, J = 4.3 Hz, 1H), 7.59 (s, 1H), 7.57–7.51 (m, 2H), 4.05 (d, J = 3.7 Hz, 2H), 4.02–3.90 (m, 3H), 3.72 (dd, J = 13.0, 5.1 Hz, 1H), 3.61–3.53 (m, 4H, overlapped with solvent peak), 3.25–3.14 (m, 1H), 2.89–2.73 (m, 2H), 2.70–2.58 (m, 2H), 1.90–1.81 (m, 2H), 1.78–1.68 (m, 2H). HRMS (ESI) calculated for $[M+H]^+/C_{20}H_{25}F_3N_3O_3^+$: 412.1843 m/z, found: 412.1850 m/z.

tert-Butyl 3-((2-(trifluoromethyl)phenyl)ethynyl)azetidine-1-carboxylate (**13b**). The procedure described for the synthesis of **8b** was applied to **13a** (151 mg, 0.56 mmol), *tert*-butyl 3-ethynylazetidine-1-carboxylate (100 mg, 0.55 mmol), copper(I) iodide (11.4 mg, 0.06 mmol), $Pd(PPh_3)_2Cl_2$ (75.0 mg, 0.11 mmol) and trimethylamine (0.2 mL, 1.43 mmol) in MeCN (2 mL) to give the desired product as an off-white solid (110 mg, 59% yield). ^{1}H NMR (400 MHz, DMSO-d_6) δ 7.79–7.68 (m, 3H), 7.61–7.57 (m, 1H), 4.22–4.18 (m, 2H), 3.85–3.82 (m, 2H), 3.74–3.69 (m, 1H), 1.39 (s, 9H). LC-MS (ESI): m/z = 269.9 [M-*t*Bu + H]$^+$.

tert-Butyl 3-(2-(trifluoromethyl)phenethyl)azetidine-1-carboxylate (**13c**). The procedure described for the synthesis of **4c** was applied to **13b** (97.0 mg, 0.30 mmol) and 10% Pd/C (30.0 mg, 0.03 mmol) in methanol (2 mL) to give the desired product as a colorless oil (68 mg, 59% yield). ^{1}H NMR (400 MHz, Methanol-d_4) δ 7.65 (d, J = 7.9 Hz, 1H), 7.60–7.54 (m, 1H), 7.46 (d, J = 7.7 Hz, 1H), 7.38 (t, J = 7.7 Hz, 1H), 4.08–3.96 (m, 2H), 3.61–3.48 (m, 2H), 2.87–2.70 (m, 2H), 2.70–2.55

(m, 1H), 2.06–1.82 (m, 2H), 1.45 (s, 9H). LC-MS (ESI): $m/z = 274.4$ [M-*t*Bu + H]$^+$.

3-(2-(Trifluoromethyl)phenethyl)azetidine 2,2,2-trifluoroacetate (**13d**). The procedure described for the synthesis of **4d** was applied to **13c** (60.0 mg, 0.18 mmol) and trifluoroacetic acid (0.10 mL, 1.30 mmol) in 1 mL DCM. A crude product was obtained and directly applied in the next step without any further purification. LC-MS (ESI): $m/z = 230.0$ [M+H]$^+$.

(4a*R*,8a*S*)-6-(3-(2-(Trifluoromethyl)phenethyl)azetidine-1-carbony l)hexahydro-2*H*-pyrido[4,3-b][1,4]oxazin-3(4*H*)-one (**13**). The procedure described for the synthesis of **4** was applied to **15** (46.8 mg, 0.15 mmol), **13d** (50.0 mg, 0.15 mmol) and DIPEA (0.15 mL, 0.85 mmol) in MeCN (2 mL). The crude was purified by preparative HPLC (column: Phenomenex Synergi C18 150 × 25 mm, 10 μm, mobile phase: A/B = 0.1%TFA in water/acetonitrile, condition: 27 mL/min, A/B from 64/36 to 24/66) and then lyophilized to give the desired product as a colorless oil (30 mg, 49% yield). ^{1}H NMR (600 MHz, Chloroform-*d*) δ 7.62 (d, J = 7.6 Hz, 1H), 7.50–7.44 (m, 1H), 7.30 (d, J = 7.8 Hz, 1H), 7.30–7.28 (m, 1H), 6.21 (br d, J = 3.0 Hz, 1H, -NHCO-), 4.35–4.26 (m, 1H), 4.22–4.16 (m, 1H), 4.10 (t, J = 8.3 Hz, 1H), 3.97 (br d, J = 2.8 Hz, 1H), 3.88 (dd, J = 13.1, 4.9 Hz, 1H), 3.65 (dd, J = 8.3, 5.8 Hz, 1H), 3.60 (dd, J = 8.3, 5.8 Hz, 1H), 3.51–3.45 (m, 1H), 3.42–3.36 (m, 1H), 3.02–3.11 (m, 2H), 2.75–2.70 (m, 2H), 2.64–2.58 (m, 1H), 1.95–1.88 (m, 3H), 1.84–1.75 (m, 2H). ^{13}C NMR (151 MHz, Chloroform-*d*) δ 168.67, 162.64, 140.46, 132.19, 131.30, 128.74 (q, J_{C-F} = 29.7 Hz), 126.55, 126.41 (q, J_{C-F} = 5.7 Hz), 124.94 (q, J_{C-F} = 273.8 Hz), 69.84, 67.99, 56.97, 49.95, 46.52, 40.06, 36.80, 30.43, 29.92, 29.58. HRMS (ESI) calculated for [M+H]$^+$/$C_{20}H_{25}F_3N_3O_3^+$: 412.1843 m/z, found: 412.1847 m/z.

Procedure C. Diethyl (2-fluoro-4-(trifluoromethyl)benzyl)phosphonate (**5b**). To an ice-cold solution of **5a** (530 mg, 2.73 mmol) in triethyl phosphite (1.17 mL, 6.82 mmol) was added iodine (693 mg, 2.73 mmol). After stirring at room temperature overnight, the crude was purified by silica gel chromatography on a 80 g column using a medium pressure liquid chromatography (MPLC) system eluting with a gradient of *n*-heptane: ethyl acetate (100 : 0 to 0 : 100) to get the desired compound as a colorless oil (85 mg, 10%). ^{1}H NMR (300 MHz, Chloroform-*d*) δ 7.56–7.47 (m, 1H), 7.42–7.30 (m, 2H), 4.18–3.99 (m, 4H), 3.24 (d, J = 22.0 Hz, 2H), 1.28 (t, J = 7.0 Hz, 6H). LC-MS (ESI): $m/z = 315.2$ [M+H]$^+$.

tert-Butyl 3-(2-fluoro-4-(trifluoromethyl)styryl)azetidine-1-carboxylate (**5c**). To an ice-cold solution of **5b** (160 mg, 0.51 mmol) in THF (1 mL), sodium hydride (55% in mineral oil, 22.2 mg, 0.51 mmol) was added. After stirring at 0 °C for 30 min, *tert*-butyl 3-formylazetidine-1-carboxylate (94.3 mg, 0.51 mmol) in THF (0.5 mL) was added to the mixture dropwise. The reaction was stirred at room temperature overnight. A mixture of H_2O/ethyl acetate was added to quench the reaction. The organic layer was separated, washed once with brine, and dried over $MgSO_4$. After filtration, the solvent was evaporated. The compound was purified by silica gel chromatography on a 4 g column using an MPLC system eluting with a gradient of *n*-heptane/ethyl acetate (100 : 0 to 50 : 50) to get the desired compound as a colorless oil (123 mg, 70%). ^{1}H NMR (300 MHz, DMSO-d_6) δ 7.95–7.81 (m, 1H), 7.66 (d, J = 10.8 Hz, 1H), 7.56 (d, J = 8.2 Hz, 1H), 6.91–6.75 (m, 1H), 6.69–6.51 (m, 1H), 4.11–4.01 (m, 2H), 3.83–3.73 (m, 2H), 3.56–3.40 (m, 1H), 1.39 (s, 9H). MS (ESI): $m/z = 290.1$ [M-*t*Bu + H]$^+$.

tert-Butyl 3-(2-fluoro-4-(trifluoromethyl)phenethyl)azetidine-1-carboxylate (**5d**). To a solution of **5c** (120 mg, 0.35 mmol) in EtOAc (1 mL) and MeOH (1 mL), 10% Pd/C (12.0 mg, 0.01 mmol) was added. The mixture was stirred under a hydrogen atmosphere at room temperature for 30 min. The suspension was filtered to get the desired compound as a colorless oil (111 mg, 92%). ^{1}H NMR (300 MHz, DMSO-d_6) δ 7.65–7.44 (m, 3H), 3.94–3.78 (m, 2H), 3.50–3.41 (m, 2H), 2.74–2.57 (m, 2H), 2.45–2.31 (m, 1H), 1.83 (q, J = 7.7 Hz, 2H), 1.36 (s, 9H). MS (ESI): m/z = 292.2 [M-*t*Bu + H]$^+$.

3-(2-Fluoro-4-(trifluoromethyl)phenethyl)azetidine 4-methylbenzenesulfonate (**5e**). To a solution of **5d** (111 mg, 0.32 mmol) in EtOAc (1.20 mL), 4-methylbenzenesulfonic acid monohydrate (66.0 mg, 0.38 mmol) was added. The mixture was heated at reflux for 1 h. The clear, colorless solution was allowed to cool down to room temperature. The suspension was filtered, and washed with a small volume of EtOAc to get a crude product as a colorless solid, which was used in the next step without any further purification. MS (ESI): $m/z = 248.2$ [M-TsOH + H]$^+$.

(4a*R*,8a*S*)-6-(3-(2-Fluoro-4-(trifluoromethyl)phenethyl)azetidine-1-carbonyl)hexahydro-2*H*-pyrido[4,3-b][1,4]oxazin-3(4*H*)-one (**5**). The procedure described for the synthesis of **1** was applied to **15** (45.0 mg, 0.14 mmol), DIPEA (73.4 μL, 0.42 mmol) and **5e** (58.7 mg, 0.14 mmol) to yield the desired product as a colorless solid (50 mg, 83%). ^{1}H NMR (600 MHz, Chloroform-*d*) δ 7.48–7.45 (m, 1H), 7.39–7.34 (m, 1H), 7.16 (t, J = 7.7 Hz, 1H), 6.30 (br d, J = 3.0 Hz, 1H, -NHCO-), 4.32–4.28 (m, 1H), 4.21–4.17 (m, 1H), 4.09 (t, J = 8.3 Hz, 1H), 4.02 (t, J = 8.3 Hz, 1H), 3.96 (s, 1H), 3.88 (dd, J = 13.0, 4.9 Hz, 1H), 3.65 (dd, J = 8.3, 5.9 Hz, 1H), 3.59 (dd, J = 8.2, 5.9 Hz, 1H), 3.49–3.45 (m, 1H), 3.42–3.37 (m, 1H), 3.14–2.99 (m, 2H), 2.66 (t, J = 7.6 Hz, 2H), 2.60–2.55 (m, 1H), 1.95–1.90 (m, 3H), 1.81–1.75 (m, 1H). ^{13}C NMR (151 MHz, Chloroform-*d*) δ 168.37, 162.29, 157.99 (d, J_{C-F} = 254.6 Hz), 134.47 (d, J_{C-F} = 5.4 Hz), 129.85 (d, J_{C-F} = 15.4 Hz), 125.16 (q, J_{C-F} = 4.4 Hz), 123.95 (d, J_{C-F} = 4.4 Hz), 122.71 (q, J_{C-F} = 272.3 Hz), 118.50, 69.48, 67.66, 56.57, 49.58, 46.17, 39.74, 34.72, 29.59, 28.94, 26.32. HRMS (ESI) calculated for [M+H]$^+$/$C_{20}H_{24}F_4N_3O_3^+$: 430.1748 m/z, found: 430.1753 m/z.

Procedure D. (2-Fluoro-6-methoxybenzyl)triphenylphosphonium (**9b**). A solution of **9a** (202 mg, 0.93 mmol) and triphenylphosphine (242 mg, 0.92 mmol) in toluene (5 mL) was heated under reflux to 85 °C whilst vigorously stirring for 16 h. After cooling down to the room temperature, the resulting precipitate was collected by vacuum filtration and washed with toluene and hexane. The residue was resolved in chloroform and dried *in vacuo* to obtain the title compound as a white foamy solid (449 mg, 100%). ^{1}H NMR (400 MHz, Chloroform-*d*) δ 7.83–7.74 (m, 3H), 7.73–7.58 (m, 12H), 7.18–7.07 (m, 1H), 6.87 (d, J = 7.6 Hz, 1H), 6.64 (t, J = 9.0 Hz, 1H), 5.30 (dd, J = 13.9, 2.0 Hz, 2H), 2.06 (s, 3H). ^{13}C NMR (101 MHz, $CDCl_3$) δ 141.81, 135.48, 134.68 (d, J_{C-P} = 10.9 Hz), 130.54, 130.40, 127.15, 118.56, 117.71, 113.31, 113.09, 24.59 (d, J_{C-P} = 48.3 Hz), 20.93. ^{19}F NMR (376 MHz, Chloroform-*d*) δ −110.94. ^{31}P NMR (162 MHz, Chloroform-*d*) δ 21.22. HRMS (ESI) calculated for [M+H]$^+$/$C_{26}H_{23}FP^+$: 385.1516 m/z, found: 385.1517 m/z.

tert-Butyl 3-(2-fluoro-6-methoxystyryl)azetidine-1-carboxylate (**9c**). Compound **9b** (421 mg, 1.05 mmol) was added into a dry reaction vessel under N_2. After dissolving in anhydrous DCM (6 mL), 1 M sodium bis (trimethylsilyl)amide in THF (1.1 mL) was added at 0 °C and the reaction was stirred for 30 min *tert*-Butyl 3-formylazetidine-1-carboxylate (168 mg, 0.91 mmol) was added dropwise to the solution, and then the reaction mixture was stirred at room temperature for 17 h. The solvent was removed *in vacuo*, and the residue was suspended in a mixture of ethyl acetate/saturated $NaHCO_3$ (v/v = 1/1, total volume: 40 mL) and extracted with ethyl acetate (30 mL × 3). The combined organic phases were washed with saturated NaCl solution (140 mL) and dried over $MgSO_4$. After filtration and evaporation, the crude was purified by column chromatography (SiO_2, petroleum ether: ethyl acetate = 10:1 to 5:1) to obtain the desired product as a clear yellow oil (94 mg, 34%). ^{1}H NMR (400 MHz, Chloroform-*d*) δ 7.24–7.16 and 7.16–7.08 (m, 1H), 6.73–6.70 and 6.70–6.51 (m overlapped, 2H), 6.70–6.51 and 6.26–6.04 (m overlapped, 2H), 4.16 and 4.09 (t, J = 8.5 Hz, 2H), 3.86 and 3.82 (s overlapped, 3H), 3.84 and 3.73 (dd overlapped, J = 8.6, 5.7 Hz, 2H), 3.42–3.29 and 3.26–3.14 (m, 1H), 1.45 and 1.43 (s, 9H). ^{19}F NMR (376 MHz, Chloroform-*d*) δ −113.06 and −114.48. HRMS (ESI)

calculated for $[M+Na]^+/C_{17}H_{22}FNNaO_3^+$: 330.1476 m/z, found: 330.1476 m/z.

tert-Butyl 3-(2-fluoro-6-methoxyphenethyl)azetidine-1-carboxylate (**9d**). The procedure described for the synthesis of **4c** was applied to **9c** (184 mg, 0.60 mmol) and 10% Pd/C (28.5 mg, 0.03 mmol) in methanol (5 mL) to obtain the desired product as a clear colorless oil (112 mg, 60%). ^{1}H NMR (400 MHz, Chloroform-*d*) δ 7.15–7.05 (m, 1H), 6.69–6.59 (m, 2H), 3.95 (t, J = 8.3 Hz, 2H), 3.81 (s, 3H), 3.53 (dd, J = 8.5, 5.5 Hz, 2H), 2.65–2.56 (m, 2H), 2.53–2.37 (m, 1H), 1.81 (q, J = 7.5 Hz, 2H), 1.43 (s, 9H). ^{19}F NMR (376 MHz, Chloroform-*d*) δ −117.96. HRMS (ESI) calculated for $[M+Na]^+/C_{17}H_{24}FNNaO_3^+$: 332.1632 m/z, found: 332.1631 m/z.

3-(2-Fluoro-6-methoxyphenethyl)azetidine 2,2,2-trifluoroacetate (**9e**) The procedure described for the synthesis of **4d** was applied to **9d** (110 mg, 0.36 mmol) and trifluoroacetic acid (0.30 mL, 4.27 mmol) to give a crude product, which was directly applied to the next step. LC-MS (ESI): m/z = 210 $[M+H]^+$.

(4a*R*,8a*S*)-6-(3-(2-Fluoro-6-methoxyphenethyl)azetidine-1-carbonyl)hexahydro-2*H*-pyrido[4,3-b][1,4]oxazin-3(4*H*)-one (**9**). The procedure described for the synthesis of **4** was applied to **15** (28.0 mg, 0.09 mmol), **9e** (30.0 mg, 0.09 mmol) and DIPEA (0.10 mL, 0.57 mmol) in MeCN (2 mL). The crude was purified by preparative HPLC (column: Phenomenex Luna C18 150 × 25 mm, 10 μm, mobile phase: A/B = 0.1% TFA in water/acetonitrile, condition: 25 mL/min, A/B from 71/29 to 41/59) and then lyophilized to give the desired product as a colorless oil (17 mg, 44% yield). ^{1}H NMR (600 MHz, Chloroform-*d*) δ 7.12 (td, J = 8.3, 6.8 Hz, 1H), 6.71–6.59 (m, 2H), 6.05 (br d, J = 2.5 Hz, 1H, -NHCO-), 4.32–4.28 (m, 1H), 4.21–4.18 (m, 1H), 4.05 (t, J = 8.3 Hz, 1H), 3.99 (t, J = 8.3 Hz, 1H), 3.97 (br d, J = 2.8 Hz, 1H), 3.89–3.85 (m, 1H), 3.82 (s, 3H), 3.63 (dd, J = 8.2, 6.0 Hz, 1H), 3.58 (dd, J = 8.3, 5.9 Hz, 1H), 3.51–3.46 (m, 1H), 3.42–3.37 (m, 1H), 3.11–3.01 (m, 2H), 2.64–2.60 (m, 2H), 2.55–2.51 (m, 1H), 1.93–1.89 (m, 1H), 1.85–1.81 (m, 2H), 1.80–1.76 (m, 1H). ^{13}C NMR (151 MHz, Chloroform-*d*) δ 168.28, 162.32, 161.60 (d, J_{C-F} = 242.5 Hz), 158.59, 127.29 (d, J_{C-F} = 10.7 Hz), 116.92 (d, J_{C-F} = 18.7 Hz), 107.76 (d, J_{C-F} = 23.3 Hz), 105.95, 69.53, 67.65, 56.85, 55.81, 49.64, 46.18, 39.68, 33.81, 29.56, 29.07, 19.87. HRMS (ESI) calculated for $[M+H]^+/C_{20}H_{27}FN_3O_4^+$: 392.1980 m/z, found: 392.1983 m/z.

(2-Fluoro-6-methylbenzyl)triphenylphosphonium (**10b**). The procedure described for the synthesis of **9b** was applied to **10a** (200 mg, 0.98 mmol) and triphenylphosphine (260 mg, 0.98 mmol) in toluene (5 mL) to obtain the desired product as a foamy white solid (243 mg, 65%). ^{1}H NMR (400 MHz, Chloroform-*d*): δ 7.87–7.76 (m, 3H), 7.71–7.57 (m, 12H), 7.25–7.18 (m, 1H), 6.57 (t, J = 8.4 Hz, 1H), 6.49 (d, J = 8.4 Hz, 1H), 4.85 (d, J = 13.6 Hz, 2H), 3.38 (s, 3H). ^{13}C NMR (100 MHz, Chloroform-*d*) δ 135.58, 134.31 (d, J_{C-P} = 10.7 Hz), 131.51, 131.40, 130.49 (d, J_{C-P} = 13.5 Hz), 118.46, 117.61, 108.53, 108.32, 107.00, 56.14, 21.36 (d, J_{C-P} = 51.6 Hz). ^{19}F NMR (376 MHz, Chloroform-*d*) δ −111.94. ^{31}P NMR (162 MHz, Chloroform-*d*) δ 21.17. HRMS (ESI) calculated for $[M+H]^+/C_{26}H_{23}FOP^+$: 401.1465 m/z, found: 401.1465 m/z.

tert-Butyl 3-(2-fluoro-6-methylstyryl)azetidine-1-carboxylate (**10c**). Compound **10c** was synthesized by following the procedure for compound **9c** using **10b** (400 mg, 1.04 mmol), *tert*-butyl 3-formylazetidine-1-carboxylate (173 mg, 0.94 mmol) and 1 M sodium bis(trimethylsilyl) amide (1.14 mL, 1.14 mmol). The desired product was obtained as a yellow oil (233 mg, 39%). ^{1}H NMR (400 MHz, Chloroform-*d*): δ 7.17–7.02 (m, 1H), 6.99–6.84 (m, 2H), 6.47–6.30 and 6.24–6.06 (m, 2H), 4.18 and 4.07 (t, J = 8.6 Hz, 2H), 3.84 and 3.72 (dd, J = 8.6, 5.9 Hz, 2H), 3.44–3.30 and 3.21–3.07 (m, 1H), 2.34 and 2.21 (s, 3H), 1.45 and 1.43 (s, 9H). ^{19}F NMR (376 MHz, Chloroform-*d*) δ −114.62 and −115.24. HRMS (ESI) calculated for $[M+Na]^+/C_{17}H_{22}FNNaO_2^+$: 314.1527 m/z, found: 314.1527 m/z.

tert-Butyl 3-(2-fluoro-6-methylphenethyl)azetidine-1-carboxylate (**10d**). The procedure described for the synthesis of **4c** was applied to **10c** (377 mg, 1.30 mmol) and 10% Pd/C (60.6 mg, 0.06 mmol) in methanol (5 mL) to obtain the title compound as a yellow oil (370 mg, 98%). ^{1}H NMR (400 MHz, Chloroform-*d*) δ 7.11–7.01 (m, 1H), 6.92 (d, J = 7.5 Hz, 1H), 6.90–6.81 (m, 1H), 4.00 (t, J = 8.5 Hz, 2H), 3.54 (dd, J = 8.6, 5.5 Hz, 2H), 2.65–2.56 (m, 2H), 2.57–2.43 (m, 1H), 2.31 (s, 3H), 1.87–1.76 (m, 2H), 1.43 (s, 9H). ^{13}C NMR (101 MHz, Chloroform-*d*) δ 161.71 (d, J_{C-F} = 243.1 Hz), 156.75, 138.63, 127.28 (d, J_{C-F} = 10.5 Hz), 127.05, 126.09, 113.06 (d, J_{C-F} = 23.8 Hz), 79.55, 54.76, 34.27, 29.00, 28.77, 23.35, 19.39. ^{19}F NMR (376 MHz, Chloroform-*d*) δ −118.77. HRMS (ESI) calculated for $[M+Na]^+/C_{17}H_{24}FNNaO_2^+$: 316.1683 m/z, found: 316.1682 m/z.

3-(2-Fluoro-6-methylphenethyl)azetidine 2,2,2-trifluoroacetate (**10e**). The procedure described for the synthesis of **4d** was applied to **10d** (100 mg, 0.341 mmol) and trifluoroacetic acid (0.30 mL, 4.09 mmol) to give a crude product, which was directly applied in the next step. LC-MS (ESI): m/z = 194 $[M+H]^+$.

(4a*R*,8a*S*)-6-(3-(2-Fluoro-6-methylphenethyl)azetidine-1-carbonyl) hexahydro-2*H*-pyrido[4,3-b][1,4]oxazin-3(4*H*)-one (**10**). The procedure described for the synthesis of **4** was applied to **15** (32 mg, 0.10 mmol), **10e** (30.0 mg, 0.10 mmol) and DIPEA (0.10 mL, 0.57 mmol) in MeCN (2 mL). The crude was purified by preparative HPLC (column: Unisil 3–100C18 Ultra 150 × 50 mm, 3 μm, mobile phase: A/B = 0.225% formic acid in water/acetonitrile, condition: 25 mL/min, A/B from 65/35 to 45/55) and then lyophilized to the desired product as a colorless oil (16 mg, 44% yield). ^{1}H NMR (600 MHz, Chloroform-*d*) δ 7.12–7.01 (m, 1H), 6.93 (d, J = 7.6 Hz, 1H), 6.86 (t, J = 8.9 Hz, 1H), 6.01 (br d, J = 0.8 Hz, 1H, -NHCO-), 4.36–4.27 (m, 1H), 4.23–4.14 (m, 1H), 4.08 (t, J = 8.3 Hz, 1H), 4.03 (t, J = 8.2 Hz, 1H), 3.97 (br d, J = 2.6 Hz, 1H), 3.87 (br dd, J = 13.0, 4.5 Hz, 1H), 3.64 (dd, J = 8.2, 5.9 Hz, 1H), 3.58 (dd, J = 8.2, 5.9 Hz, 1H), 3.52–3.45 (m, 1H), 3.43–3.37 (m, 1H), 3.14–2.90 (m, 2H), 2.68–2.39 (m, 3H), 2.32 (s, 3H), 1.91 (dd, J = 14.4, 2.7 Hz, 1H), 1.85–1.71 (m, 3H).^{13}C NMR (151 MHz, Chloroform-*d*) δ 168.20, 162.14, 161.42 (d, J_{C-F} = 267.6 Hz), 138.31, 127.00, 126.65, 125.78, 112.71 (d, J_{C-F} = 23.4 Hz), 69.52, 67.68, 56.76, 49.64, 46.18, 39.69, 33.98, 29.57, 29.18, 22.96, 19.06. HRMS (ESI) calculated for $[M+H]^+/C_{20}H_{27}FN_3O_3^+$: 376.2031 m/z, found: 376.2037 m/z.

(2,6-Difluorobenzyl)triphenylphosphonium (**11b**). The procedure described for the synthesis of **9b** was applied to **11a** (100 mg, 0.49 mmol) and triphenylphosphine (127 mg, 0.49 mmol) in toluene (5 mL) to obtain the desired product as a white solid (150 mg, 78%). ^{1}H NMR (400 MHz, Chloroform-*d*): δ 7.84–7.71 (m, 9H), 7.70–7.60 (m, 6H), 7.25–7.20 (m, 1H), 6.78–6.67 (m, 2H), 5.31 (d, J = 14.0 Hz, 2H). ^{13}C NMR (101 MHz, Chloroform-*d*) δ 135.63, 134.45 (d, J_{C-P} = 10.7 Hz), 131.42, 130.57 (d, J_{C-P} = 13.9 Hz), 118.15, 117.31, 112.21, 111.98, 21.49 (d, J_{C-P} = 51.3 Hz). ^{19}F NMR (376 MHz, Chloroform-*d*) δ −108.88. ^{31}P NMR (162 MHz, $CDCl_3$) δ 22.24. HRMS (ESI) calculated for $[M+H]^+/C_{25}H_{20}F_2P^+$: 389.1265 m/z, found: 389.1270 m/z.

tert-Butyl 3-(2,6-difluorostyryl)azetidine-1-carboxylate (**11c**). Compound **11c** was synthesized by following the procedure for compound **9c** using **11b** (700 mg, 1.80 mmol), *tert*-butyl 3-formylazetidine-1-carboxylate (333.2 mg, 1.799 mmol) and 1 M sodium bis(trimethylsilyl) amide (2.16 mL, 2.16 mmol). The desired product was obtained as a yellow oil (413 mg, 72%). ^{1}H NMR (400 MHz, Chloroform-*d*) δ 7.25–7.18 and 7.18–7.07 (m, 1H), 6.92–6.82 and 6.89–6.84 (m overlapped, 2H), 6.70 and 6.16 (dd overlapped, J = 16.2, 8.4 Hz, 1H), 6.44 and 6.22 (d overlapped, J = 16.2 Hz, 1H), 4.17 and 4.12 (t, J = 8.5 Hz, 2H), 3.84 and 3.74 (dd, J = 8.6, 5.9 Hz, 2H), 3.43–3.29 and 3.29–3.15 (m, 1H), 1.45 and 1.43 (s, 9H). ^{19}F NMR (376 MHz, Chloroform-*d*) δ −111.79 and −113.56. HRMS (ESI): Calculated for $[M+Na]^+/C_{16}H_{19}F_2NNaO_2^+$: 318.1276 m/z, found: 318.1276 m/z.

tert-Butyl 3-(2,6-difluorophenethyl)azetidine-1-carboxylate (**11d**). The procedure described for the synthesis of **4c** was applied to **11c** (413 mg, 1.40 mmol) and 10% Pd/C (65.6 mg, 0.06 mmol) in methanol (5 mL) to obtain the desired product as a colorless oil (350 mg, 84%). ^{1}H NMR (400 MHz, Chloroform-*d*) δ 7.19–7.08 (m, 1H), 6.89–6.78 (m, 2H), 3.98 (t, J = 8.4 Hz, 2H), 3.54 (dd, J = 8.6, 5.5 Hz, 2H), 2.64 (t, J = 7.0 Hz, 2H), 2.54–2.42 (m, 1H), 1.87 (q, J = 7.6 Hz, 2H), 1.43 (s, 9H). ^{13}C

NMR (100 MHz, Chloroform-*d*) δ 161.89 (d, J_{C-F} = 247.5 Hz), 161.79 (d, J_{C-F} = 247.4 Hz), 156.71, 127.92 (t, J_{C-F} = 10.7 Hz), 117.12 (t, J_{C-F} = 20.6 Hz), 111.38 (d, J_{C-F} = 28.6 Hz), 79.53, 54.65, 34.24, 28.37, 20.06. ^{19}F NMR (376 MHz, Chloroform-*d*) δ −116.32. HRMS (ESI): Calculated for $[M+Na]^+/C_{16}H_{21}F_2NNaO_2^+$: 320.1433 m/z, found: 320.1436 m/z.

3-(2,6-Difluorophenethyl)azetidine 2,2,2-trifluoroacetate (**11e**). The procedure described for the synthesis of **4d** was applied to **11d** (60.0 mg, 0.20 mmol) and trifluoroacetic acid (0.11 mL, 1.44 mmol) to give a crude product, which was directly applied to the next step. LC-MS (ESI): *m/z* = 198.5 $[M+H]^+$.

(4a*R*,8a*S*)-6-(3-(2,6-Difluorophenethyl)azetidine-1-carbonyl)hexahydro-2*H*-pyrido[4,3-b][1,4]oxazin-3(4*H*)-one (**11**). The procedure described for the synthesis of **4** was applied to **15** (43.4 mg, 0.13 mmol), **11e** (42.0 mg, 0.13 mmol) and DIPEA (0.14 mL, 0.79 mmol) in MeCN (2 mL). The crude was purified by preparative HPLC (column: Phenomenex Synergi C18 150 × 25 mm, 10 μm, mobile phase: A/B = 0.1%TFA in water/acetonitrile, condition: 27 ml/min, A/B from 70/30 to 40/60) and then lyophilized to give the desired product as a colorless oil (33 mg, 60% yield). ^{1}H NMR (400 MHz, DMSO-d_6) δ 8.14 (d, *J* = 3.8 Hz, 1H, -NHCO-), 7.37–7.26 (m, 1H), 7.12–7.03 (m, 2H), 4.09–4.00 (m, 2H), 3.99–3.94 (m, 1H), 3.92 (d, *J* = 8.2 Hz, 2H), 3.70 (dd, *J* = 4.5, 12.6 Hz, 1H), 3.55 (br s, 4H), 3.20 (d, *J* = 8.3 Hz, 1H), 2.85–2.74 (m, 2H), 2.62–2.58 (m, 2H), 1.83–1.70 (m, 4H). HRMS (ESI) calculated for $[M+H]^+/C_{19}H_{24}F_2N_3O_3^+$: 380.1780 m/z, found: 380.1785 m/z.

(2-Fluorobenzyl)triphenylphosphonium (**12b**).The procedure described for the synthesis of **9b** was applied to **12a** (2.00 g, 10.6 mmol) and triphenylphosphine (2.79 g, 10.6 mmol) in toluene (5 mL) to obtain the desired product as a white solid (539 mg, 92%). ^{1}H NMR (400 MHz, Chloroform-*d*): δ 7.88–7.73 (m, 9H), 7.71–7.63 (m, 6H), 7.61–7.53 (m, 1H), 7.27–7.21 (m, 1H), 7.03 (t, *J* = 7.6 Hz, 1H), 6.88–6.79 (m, 1H), 5.55 (d, *J* = 14.3 Hz, 2H). ^{13}C NMR (101 MHz, Chloroform-*d*) δ 135.40, 134.61 (d, J_{C-P} = 10.7 Hz), 134.13, 130.89, 130.49 (d, J_{C-P} = 14.0 Hz), 125.33, 118.43, 117.58, 115.60 (d, J_{C-F} = 23.6 Hz), 24.88 (d, J_{C-P} = 49.2 Hz). ^{19}F NMR (376 MHz, Chloroform-*d*) δ −115.05. ^{31}P NMR (162 MHz, Chloroform-*d*) δ 22.93. HRMS (ESI) calculated for $[M+H]^+/C_{25}H_{21}FP^+$: 371.1359 m/z, found: 371.1361 m/z.

tert-Butyl 3-(2-fluorostyryl)azetidine-1-carboxylate (**12c**). Compound **12c** was synthesized by following the procedure for compound **9c** using **12b** (150 mg, 0.40 mmol), *tert*-butyl 3-formylazetidine-1-carboxylate (75.0 mg, 0.40 mmol) and 1 M sodium bis(trimethylsilyl)amide (0.49 mL, 0.49 mmol). The desired product was obtained as a yellow oil (61 mg, 55%). ^{1}H NMR (400 MHz, Chloroform-*d*) δ 7.48–7.39 and 7.28–7.22 (m overlapped, 1H), 7.22–7.16 and 7.12–7.00 (m overlapped, 3H), 6.58 and 6.49 (d overlapped, *J* = 16.0 Hz, 1H), 6.44 and 6.03 (dd overlapped, *J* = 11.3, 9.3 Hz, 1H), 4.17 and 4.13 (t, *J* = 7.6 Hz, 2H), 3.83 and 3.75 (dd, *J* = 8.6, 5.9 Hz, 2H), 3.58–3.43 and 3.43–3.31 (m, 1H), 1.45 and 1.44 (s, 9H). ^{19}F NMR (376 MHz, Chloroform-*d*) δ −108.87 and −108.88. HRMS (ESI) calculated for $[M+Na]^+/C_{16}H_{20}FNNaO_2^+$: 300.1370 m/z, found: 300.1375 m/z.

tert-Butyl 3-(2-fluorophenethyl)azetidine-1-carboxylate (**12d**). The procedure described for the synthesis of **4c** was applied to **12c** (61.2 mg, 0.22 mmol) and 10% Pd/C (10.4 mg, 0.01 mmol) in methanol (5 mL) to obtain the title compound as a colorless oil (36 mg, 58%). ^{1}H NMR (400 MHz, Chloroform-*d*) δ 7.23–7.09 (m, 2H), 7.09–6.95 (m, 2H), 3.98 (t, *J* = 8.5 Hz, 2H), 3.54 (dd, *J* = 8.6, 5.5 Hz, 2H), 2.60 (t, *J* = 7.5 Hz, 2H), 2.56–2.42 (m, 1H), 1.95–1.84 (m, 2H), 1.43 (s, 9H). ^{13}C NMR (101 MHz, Chloroform-*d*) δ 161.11 (d, J_{C-F} = 245.0 Hz), 156.39, 130.55 (d, J_{C-F} = 5.7 Hz), 128.18 (d, J_{C-F} = 15.8 Hz), 127.80 (d, J_{C-F} = 8.7 Hz), 124.05, 115.28 (d, J_{C-F} = 22.8 Hz), 79.19, 54.34, 34.81, 28.42, 26.57. ^{19}F NMR (376 MHz, Chloroform-*d*) δ −119.07. HRMS (ESI) calculated for $[M+Na]^+/C_{16}H_{22}FNNaO_2^+$: 302.1527 m/z, found: 302.1530 m/z.

3-(2-Fluorophenethyl)azetidine 2,2,2-trifluoroacetate (**12e**). The procedure described for the synthesis of **4d** was applied to **12d** (62.0 mg, 0.22 mmol) and trifluoroacetic acid (0.20 mL, 2.67 mmol) to give a crude product, which was directly applied in the next step. LC-MS (ESI): *m/z* = 180 $[M+H]^+$.

(4a*R*,8a*S*)-6-(3-(2-Fluorophenethyl)azetidine-1-carbonyl)-hexahydro-2H-pyrido[4,3-b][1,4]oxazin-3(4*H*)-one (**12**). Triphosgene (37.4 mg, 0.13 mmol) was filled into a dried reaction vessel under nitrogen protection and dissolved in anhydrous DCM (1 mL) at 0 °C. A mixture of **14** (53.2 mg, 0.34 mmol) and DIPEA (88.8 μL, 0.51 mmol) in anhydrous DCM (2 mL) was added over a time period of 30 min. The stirring was continued for another 10 min at 0 °C, and a mixture of compound **4d** (94.4 mg, 0.34 mmol) and DIPEA (0.15 mL, 0.88 mmol) in anhydrous DCM (2 mL) was added. Upon completion, the reaction mixture was diluted with saturated $NaHCO_3$ and extracted three times with DCM. The combined organic phases were dried over $MgSO_4$, filtered and the evaporated *in vacuo*. The residue was purified by column chromatography (SiO_2, DCM: methanol = 100:1 to 19:1) to give the desired product as a clear colorless oil (17.3 mg, 14%). ^{1}H NMR (400 MHz, Chloroform-*d*) δ 7.22–7.11 (m, 2H), 7.08–6.97 (m, 2H), 6.52–6.41 (m, 1H, -NHCO-), 4.29 (d, *J* = 16.9 Hz, 1H), 4.18 (d, *J* = 16.9 Hz, 1H), 4.05 (dt, *J* = 21.8, 8.3 Hz, 2H), 3.98–3.94 (m, 1H), 3.92–3.85 (m, 1H), 3.69–3.57 (m, 2H), 3.54–3.45 (m, 1H), 3.44–3.37 (m, 1H), 3.13–2.98 (m, 2H), 2.64–2.57 (m, 3H), 1.94–1.87 (m, 3H), 1.85–1.71 (m, 1H). ^{13}C NMR (101 MHz, Chloroform-*d*) δ 168.71, 162.65, 160.23, 130.89 (d, J_{C-F} = 6.3 Hz), 128.42 (d, J_{C-F} = 15.6 Hz), 128.19 (d, J_{C-F} = 8.5 Hz), 124.44, 115.61 (d, J_{C-F} = 22.9 Hz), 69.81, 67.99, 57.01, 49.86, 46.51, 40.01, 35.21, 29.93, 29.29, 26.87. ^{19}F NMR (376 MHz, Chloroform-*d*) δ −119.04. HRMS (ESI) calculated for $[M+H]^+/C_{19}H_{25}FN_3O_3^+$: 362.1874 m/z, found: 362.1875 m/z.

5.2. MAGL IC_{50} measurement

The IC_{50} values of compounds were measured using MAGL enzyme as previously described [9]. The experiments were carried out at least in triplet using mouse or human MAGL.

5.3. Metabolism

Microsomal clearance and hepatocyte clearance of the compounds were measured as previously reported [23,24].

Microsomal clearance. Commercially available pooled liver microsomes (C57BL/6J mice) were purchased from Corning Incorporated (Woburn, USA). The NADPH generating system consisted of 30 mM glucose-6-phosphate disodium salt hydrate, 10 mM NADP, 30 mM $MgCl_2{\cdot}6H_2O$ and 5 mg/mL glucose-6-phospahte dehydrogenase (Roche Diagnostics) in 0.1 M potassium phosphate buffer (pH = 7.4). The test compound was incubated at 1 μM with microsome concentrations of 0.5 mg/mL plus the cofactor NADPH in 96-well plates at 37 °C on TECAN (Tecan Group Ltd, Switzerland) equipped with Te-Shake shakers (Tecan Freedom EVO, Te-shake, orbital shaker silver) and a warming device (Tecan Group Ltd, Switzerland) at a shaking speed of 600 rpm and at 37 °C. At 1, 3, 6, 9, 15, 25, 35, and 45 min post-incubation, 40 μL solution was transferred and quenched with 120 μL acetonitrile containing 2-(8-aminotetralin-5-yl)-1,1,1,3,3,3-hexafluoro-propan-2-ol as an internal standard. Samples were then cooled and centrifuged before analysis by LC−MS/MS. Log peak area ratios (test compound/internal standard) are plotted against incubation time using a linear fit. The calculated slope is used to determine the intrinsic clearance, and expressed as μL per min per mg protein.

Hepatocyte Clearance. Pooled hepatocytes were purchased from BioreclamationIVT (NY, USA), and the cell culture medium was William's media supplemented with glutamine, antibiotics, insulin, dexamethasone and 10% fetal bovine serum. 96-well plates (Nunc Natural, 267245) were used for suspension cultures. The compound was tested at 1 μM concentration in suspension cultures of 1 million cell/mL (approx. 1 mg/mL protein centration). The 96-well plates were incubated in a Thermo Forma incubator (Fischer Scientific, Wohlen, Switzerland) up to 2 h with 5% CO_2 atmosphere at 37 °C, and shook at 900 rpm (Variomag Teleshake shaker, Sterico, Wangen, Switzerland) to maintain cell

dispersion. At 3, 6, 10, 20, 40, 60, and 120 min post-incubation, 100 μL cell suspension in each well was quenched by 200 μL methanol containing 2-(8-aminotetralin-5-yl)-1,1,1,3,3,3-hexafluoro-propan-2-ol as an internal standard. The samples were then cooled and centrifuged for LC-MS/MS analysis. Log peak area ratios (test compound/internal standard) are plotted against incubation time using a linear fit. The calculated slope is used to determine the intrinsic clearance, and expressed as μL per min per million cells.

5.4. SPR measurements

All SPR experiments were performed on the SPR instruments (Biacore 3000 and T200, GE Healthcare, Uppsala, Sweden) at 18 °C in the running buffer (10 mM HEPES, 150 mM NaCl, 0.05% (v/v) Surfactant P20, pH 7.4, 50 μM EDTA supplemented with 1% DMSO (v/v) for binding assay if desired). Protein immobilization and binding assay were performed at flow rate of 5 and 30 μL/min, respectively. The chemical structure of the reference compound and the typical binding curves in a single cycle kinetic mode are provided in the supporting information (Fig. S2).

Protein immobilization. *N*-terminally tagged, full-length mouse His6-TEV-MAGL protein was immobilized on CM5 SPR sensor (Cat. No. BR-100530, GE Healthcare, Uppsala, Sweden) applying protected amino coupling surface chemistry. The target protein was first pre-diluted 40 times from stock (2.3 mg/mL) in the running buffer and further diluted in the coupling buffer (10 mM acetate, pH 5.5) containing 10 μM reference compound to stabilize the protein while immobilization. The sensor surface was first activated by a mixture of 0.2 M 1-ethyl-3-(3-dimethylaminopropyl)-carbodiimide and 0.5 M *N*-hydroxysuccinimide for 10 min. Afterwards, the activated surface was contacted with the protein solution at final protein concentration of 0.06 mg/mL in acetate buffer in presence of the reference compound at saturating concentration until the desired protein surface density was achieved (Response: ca. 3000–4000 relative units). No deactivation of sensor surface was performed. Protein surface was prepared freshly to analyze each slow dissociating compound.

Binding assay. All samples were dissolved in DMSO to get 10 mM stock solutions. Further, the samples were diluted with running buffer to get dilution series (adapted to the affinity of the compound) and analyzed in the single cycle kinetic mode (5 concentrations with the dilution factor of 2). Injection of buffer (blank) was performed to collect buffer signal enabling further data proceeding. The protein binding activity was tested with (2-chlorophenyl)(3-(4-(pyrimidin-2-yl)piperazin-1-yl)azetidin-1-yl)methanone), a fast dissociating compound, prior to the injection of slow dissociating compounds.

Data proceeding. SPR resonance signals measured on the active channel (protein channel) were subtracted with signals collected on the reference channel (only activated sensor surface, no protein) and further subtracted with buffer signal (blank). Kinetic and binding parameters were extracted from the experimental binding curves by fitting them into mathematical binding model for one-to-one interaction applying Biacore T200 Evaluation software (version 3.2.1).

5.5. Activity-based protein profiling assay (ABPP) of compound 7

The ABPP assay was performed using a modified procedure according to the reported literature [15]. Detailed procedures are provided in the Supporting Information.

5.6. Radiosynthesis

Compound **14** (0.672 mg, 4.3 μmol), BEMP (5 μL, 17.3 μmol), 0.2% $POCl_3$ (v/v, 2.15 μmol in 100 μL MeCN) and **7d** prepared as tosylate salt (4.7 μmol in 100 μL MeCN) were employed to obtain [^{11}C]**7** using the radiolabeling method described previously [10]. Semi-preparative HPLC with a gradient method was applied for purification (ACE5 C18-300 column, 250 × 10 mm, 5 μm; mobile phase A: water containing 0.1% H_3PO_4, mobile phase B: CH_3CN; flow rate of 4 mL/min; 0.0–6.0 min, 30–50% B; 6.0–8.0 min, 50–55% B; 8.0–12.0 min, 55–60% B; 12.0–18.0 min, 60–95% B; 18.0–20.0 min, 95% B at a wavelength of 254 nm). The identification of the radioactive product was performed in an Agilent 1100 series HPLC system, equipped with UV detector and a GabiStar radiodetector (Raytest) using an ACE XDB-C18 Zobrax column (75 mm × 4.6 mm, 3.5 μm; mobile phase A: water containing 0.1% H_3PO_4, mobile phase B: CH_3CN; flow rate of 1 mL/min; 0.0–3.0 min, 30–50% B; 3.0–4.0 min, 50–55% B; 4.0–6.0 min, 55–60% B; 6.0–7.0 min, 60–70% B with a wavelength of 254/230 nm). The retention time of **7** and [^{11}C]**7** were 4.99 and 5.02 min, respectively. The difference in retention time was in agreement with the time lag between the UV and radioactivity detectors in our HPLC system. [^{11}C]**2** was synthesized according to the literature [10].

5.7. Lipophilicity and in vitro stability

The lipophilicity and *in vitro* stability of [^{11}C]**7** were measured as previously described [9].

5.8. In vitro autoradiography

The *in vitro* autoradiography of [^{11}C]**7** was carried out using an analogous procedure in the literature [10]. An aqueous buffer comprising 30 mM HEPES, 1.2 mM $MgCl_2$, 110 mM NaCl, 5 mM KCl, 2.5 mM $CaCl_2$, and 1% fatty acid free bovine serum albumin (pH ~7.4) was employed as incubation buffer. The brain sections were incubated with [^{11}C]**7** (18 nM, 65.6 GBq/μmol) in a humidified chamber for 30 min. Blocking experiments on Wistar brain sections were carried out in the presence of 10 μM SAR127303 or 10 μM PF-06795071. Upon the completion of incubation, the slices were washed in the above-mentioned incubation buffer (pH 7.4, 0 °C, 1 × 2 min), washing buffer comprising 30 mM HEPES, 1.2 mM $MgCl_2$, 110 mM NaCl, 5 mM KCl, 2.5 mM $CaCl_2$ (pH 7.4, 0 °C, 2 × 2 min), followed by 2 quick dips in distilled water (0 °C, 2 × 5 s). After drying, the slices were attached to a phosphor image plate (Fuji, Dielsdorf, Switzerland) and the exposure lasted for 60 min. The film was scanned by BAS5000 reader (Fuji), and the autoradiogram was analyzed by AIDA 4.50.010 software (Raytest Isotopenmessgeräte GmbH, Straubenhardt, Germany).

5.9. In vivo PET imaging

All animals were taken care in accordance with Swiss Animal Welfare legislation. The experiments were complied with ARRIVE guidelines and authorized by the Veterinary Office of the Canton Zurich (ZH28/2018). PET imaging was carried out in mouse under anesthesia with a Super Argus PET/CT tomograph (Sedecal, Madrid, Spain). The radiotracer (6.33–14.42 nmol/kg) was administrated *via* tail-vein injection, and dynamic PET data was acquired 1 min later. A 60 min scan protocol was applied in all animal studies. For blocking studies, MAGLi432 were injected into the mice 5 min prior to tracer injection (5 mg/kg, formulated in DMSO/Tween80/saline = 1/1/8, v/v/v). The resulting data were reconstructed in user-defined time frames with a voxel size of 0.3875 × 0.3875 × 0.775 mm^3, and the data analysis were carried out using PMOD 4.002 software (PMOD Technologies Ltd., Zurich, Switzerland) as previously described [10]. The radioactive accumulations in mice brain were expressed as standardized uptake values (SUVs), which is the decay-corrected regional radioactivity normalized to the injected radioactivity and body weight.

5.10. Radiometabolite analysis

[^{11}C]**7** was concentrated and administered intravenously *via* tail vein (~190 MBq with a radiochemical purity greater than 97%), and the animal was scarified by decapitation at 40 min post-injection. The brain

sample was collected and analyzed as previously described [10]. Briefly, the brain homogenate was obtained in 1 mL PBS buffer after dissection. After centrifugation at 4 °C for 5 min, the supernatant was taken and 1 mL ice-cold MeCN was added for protein precipitation. The mixture was centrifuged, and the resulting supernatant was passed through a 0.22 μM Nalgene PES syringe filter. Afterwards, 10 μL sample was injected to a Waters Acquity ultra-performance liquid chromatography (UPLC) equipped with BEH C18 column (Acquity Waters, 130 Å, 1.7 μm, 2.1 mm × 50 mm) and FlowStar LB 513 Radioactivity Flow Detector. A gradient method using 10 mM NH_4HCO_3 in Milli-Q water as mobile phase A and MeCN as mobile phase B was employed at the flow of 0.6 ml/min for analysis (0.0–2.0 min, 5–30% B; 2.0–3.5min, 30–50% B; 3.5–4.0 min, 50–90% B; 4.0–6.0 min, 90% B).

Declaration of competing interest

The authors declare the following financial interests/personal relationships which may be considered as potential competing interests: Yingfang He reports financial support was provided by China Scholarship Council. COLLIN LUDOVIC, EDELMANN MARTIN, GOBBI LUCA, GRETHER UWE, HE YINGFANG, HONER MICHAEL, MU LINJING, RICHTER HANS has patent RADIOLABELED COMPOUNDS issued to ETH Zurich, F. Hoffmann-La Roche Ltd.

Data availability

Data will be made available on request.

Acknowledgements

We sincerely thank Marie-Thérèse Miss (Roche Innovation Center Basel) for organizing the MAGL knockout mice and Isabelle Kaufmann (Roche Innovation Center Basel), Martin Ritter (Roche Innovation Center Basel), Dominic Flury (Roche Innovation Center Basel) for the technical assistance. Björn Wagner (Roche Innovation Center Basel) and Carina Cantrill (Roche Innovation Center Basel) are acknowledged for the determination of LIMBA LogD, PAMPA P_{eff} values, and AP-ER from P-gp *in vitro* transport experiments. The authors thank Lianshun Feng, Xiaofei Yan and the team of Wuxi AppTec for skillful synthesis support. Svenja Moes (Roche Innovation Center Basel) and Jennifer Beck (Roche Innovation Center Basel) are acknowledged for the assistance of *ex vivo* autoradiography using [^{3}H]**7** (unpublished data). Bruno Mancosu (ETH Zurich) is particularly acknowledged for building up the brilliant [^{11}C]CO_2 module for radiolabeling. Dr. Yingfang He received the generous financial support from China Scholarship Council (Project number: CSC201706040066).

Appendix B. Supplementary data

Supplementary data to this article can be found online at https://doi.org/10.1016/j.ejmech.2022.114750.

Appendix A. Supplementary data

Supplementary data to this article can be found online.

References

[1] O. Aizpurua-Olaizola, I. Elezgarai, I. Rico-Barrio, I. Zarandona, N. Etxebarria, A. Usobiaga, Targeting the endocannabinoid system: future therapeutic strategies, Drug Discov. Today 22 (2017) 105–110, https://doi.org/10.1016/j.drudis.2016.08.005.

[2] T. Ohno-Shosaku, M. Kano, Endocannabinoid-mediated retrograde modulation of synaptic transmission, Curr. Opin. Neurobiol. 29 (2014) 1–8, https://doi.org/10.1016/j.conb.2014.03.017.

[3] J.R. Piro, D.I. Benjamin, J.M. Duerr, Y.Q. Pi, C. Gonzales, K.M. Wood, J. W. Schwartz, D.K. Nomura, T.A. Samad, A dysregulated endocannabinoid-eicosanoid network supports pathogenesis in a mouse model of Alzheimer's disease, Cell Rep. 1 (2012) 617–623, https://doi.org/10.1016/j.celrep.2012.05.001.

[4] A. Gil-Ordóñez, M. Martín-Fontecha, S. Ortega-Gutiérrez, M.L. López-Rodríguez, Monoacylglycerol lipase (MAGL) as a promising therapeutic target, Biochem. Pharmacol. 157 (2018) 18–32, https://doi.org/10.1016/j.bcp.2018.07.036.

[5] N. van Egmond, V.M. Straub, M. van der Stelt, Targeting endocannabinoid signaling: FAAH and MAG lipase inhibitors, Annu. Rev. Pharmacol. Toxicol. 61 (2021) 441–463, https://doi.org/10.1146/annurev-pharmtox-030220-112741.

[6] Z. Chen, W. Mori, X. Deng, R. Cheng, D. Ogasawara, G. Zhang, M.A. Schafroth, K. Dahl, H. Fu, A. Hatori, T. Shao, Y. Zhang, T. Yamasaki, X. Zhang, J. Rong, Q. Yu, K. Hu, M. Fujinaga, L. Xie, K. Kumata, Y. Gou, J. Chen, S. Gu, L. Bao, L. Wang, T. L. Collier, N. Vasdev, Y. Shao, J.-A. Ma, B.F. Cravatt, C. Fowler, L. Josephson, M.-R. Zhang, S.H. Liang, Design, synthesis, and evaluation of reversible and irreversible monoacylglycerol lipase positron emission tomography (PET) tracers using a "tail switching" strategy on a piperazinyl azetidine skeleton, J. Med. Chem. 62 (2019) 3336–3353, https://doi.org/10.1021/acs.jmedchem.8b01778.

[7] J. Rong, W. Mori, X. Xia, M.A. Schafroth, C. Zhao, R.S. Van, T. Yamasaki, J. Chen, Z. Xiao, A. Haider, D. Ogasawara, A. Hiraishi, T. Shao, Y. Zhang, Z. Chen, F. Pang, K. Hu, L. Xie, M. Fujinaga, K. Kumata, Y. Gou, Y. Fang, S. Gu, H. Wei, L. Bao, H. Xu, T.L. Collier, Y. Shao, R.E. Carson, B.F. Cravatt, L. Wang, M.-R. Zhang, S.H. Liang, Novel reversible-binding PET ligands for imaging monoacylglycerol lipase based on the piperazinyl azetidine scaffold, J. Med. Chem. 64 (2021) 14283–14298, https://doi.org/10.1021/acs.jmedchem.1c00747.

[8] Y. Hattori, K. Aoyama, J. Maeda, N. Arimura, Y. Takahashi, M. Sasaki, M. Fujinaga, C. Seki, Y. Nagai, K. Kawamura, T. Yamasaki, M.-R. Zhang, M. Higuchi, T. Koike, Design, synthesis, and evaluation of (4*R*)-1-{3-[2-(^{18}F)Fluoro-4-methylpyridin-3-yl]phenyl}-4-[4-(1,3-thiazol-2-ylcarbonyl)piperazin-1-yl]pyrrolidin-2-one ([^{18}F]T-401) as a novel positron-emission tomography imaging agent for monoacylglycerol lipase, J. Med. Chem. 62 (2019) 2362–2375, https://doi.org/10.1021/acs.jmedchem.8b01576.

[9] Y. He, M. Schild, U. Grether, J. Benz, L. Leibrock, D. Heer, A. Topp, L. Collin, B. Kuhn, M. Wittwer, C. Keller, L.C. Gobbi, R. Schibli, L. Mu, Development of high brain-penetrant and reversible monoacylglycerol lipase PET tracers for neuroimaging, J. Med. Chem. 65 (2022) 2191–2207, https://doi.org/10.1021/acs.jmedchem.1c01706.

[10] Y. He, L.C. Gobbi, A.M. Herde, D. Rombach, M. Ritter, B. Kuhn, M.B. Wittwer, D. Heer, B. Hornsperger, C. Bell, F. O'Hara, J. Benz, M. Honer, C. Keller, L. Collin, H. Richter, R. Schibli, U. Grether, L. Mu, Discovery, synthesis and evaluation of novel reversible monoacylglycerol lipase radioligands bearing a morpholine-3-one scaffold, Nucl. Med. Biol. 108–109 (2022) 24–32, https://doi.org/10.1016/j.nucmedbio.2022.02.002.

[11] C. Granchi, I. Caligiuri, F. Minutolo, F. Rizzolio, T. Tuccinardi, A patent review of Monoacylglycerol Lipase (MAGL) inhibitors (2013-2017), Expert Opin. Ther. Pat. 27 (2017) 1341–1351, https://doi.org/10.1080/13543776.2018.1389899.

[12] G. Bononi, G. Poli, F. Rizzolio, T. Tuccinardi, M. Macchia, F. Minutolo, C. Granchi, An updated patent review of monoacylglycerol lipase (MAGL) inhibitors (2018-present), Expert Opin. Ther. Pat. 31 (2021) 153–168, https://doi.org/10.1080/13543776.2021.1841166.

[13] L. Hou, J. Rong, A. Haider, D. Ogasawara, C. Varlow, M.A. Schafroth, L. Mu, J. Gan, H. Xu, C.J. Fowler, M.-R. Zhang, N. Vasdev, S. Ametamey, B.F. Cravatt, L. Wang, S.H. Liang, Positron emission tomography imaging of the endocannabinoid system: opportunities and challenges in radiotracer development, J. Med. Chem. 64 (2021) 123–149, https://doi.org/10.1021/acs.jmedchem.0c01459.

[14] G. Labar, C. Bauvois, F. Borel, J.-L. Ferrer, J. Wouters, D.M. Lambert, Crystal structure of the human monoacylglycerol lipase, a key actor in endocannabinoid signaling, Chembiochem 11 (2010) 218–227, https://doi.org/10.1002/cbic.200900621.

[15] A.P.A. Janssen, D. van der Vliet, A.T. Bakker, M. Jiang, S.H. Grimm, G. Campiani, S. Butini, M. van der Stelt, Development of a multiplexed activity-based protein profiling assay to evaluate activity of endocannabinoid hydrolase inhibitors, ACS Chem. Biol. 13 (2018) 2406–2413, https://doi.org/10.1021/acschembio.8b00534.

[16] J.Z. Long, W. Li, L. Booker, J.J. Burston, S.G. Kinsey, J.E. Schlosburg, F.J. Pavón, A. M. Serrano, D.E. Selley, L.H. Parsons, A.H. Lichtman, B.F. Cravatt, Selective blockade of 2-arachidonoylglycerol hydrolysis produces cannabinoid behavioral effects, Nat. Chem. Biol. 5 (2009) 37–44, https://doi.org/10.1038/nchembio.129.

[17] J. Aida, M. Fushimi, T. Kusumoto, H. Sugiyama, N. Arimura, S. Ikeda, M. Sasaki, S. Sogabe, K. Aoyama, T. Koike, Design, synthesis, and evaluation of piperazinyl pyrrolidin-2-ones as a novel series of reversible monoacylglycerol lipase inhibitors, J. Med. Chem. 61 (2018) 9205–9217, https://doi.org/10.1021/acs.jmedchem.8b00824.

[18] L. Zhang, A. Villalobos, E.M. Beck, T. Bocan, T.A. Chappie, L. Chen, S. Grimwood, S.D. Heck, C.J. Helal, X. Hou, J.M. Humphrey, J. Lu, M.B. Skaddan, T.J. McCarthy, P.R. Verhoest, T.T. Wager, K. Zasadny, Design and selection parameters to accelerate the discovery of novel central nervous system positron emission tomography (PET) ligands and their application in the development of a novel phosphodiesterase 2A PET ligand, J. Med. Chem. 56 (2013) 4568–4579, https://doi.org/10.1021/jm400312y.

[19] T.P. Dinh, D. Carpenter, F.M. Leslie, T.F. Freund, I. Katona, S.L. Sensi, S. Kathuria, D. Piomelli, Brain monoglyceride lipase participating in endocannabinoid inactivation, Proc. Natl. Acad. Sci. USA 99 (2002) 10819–10824, https://doi.org/10.1073/pnas.152334899.

[20] T. Yamasaki, W. Mori, Y. Zhang, A. Hatori, M. Fujinaga, H. Wakizaka, Y. Kurihara, L. Wang, N. Nengaki, T. Ohya, S.H. Liang, M.R. Zhang, First demonstration of in vivo mapping for regional brain monoacylglycerol lipase using PET with [^{11}C]

SAR127303, Neuroimage 176 (2018) 313–320, https://doi.org/10.1016/j.neuroimage.2018.05.015.
[21] M. Honer, L. Gobbi, L. Martarello, R.A. Comley, Radioligand development for molecular imaging of the central nervous system with positron emission tomography, Drug Discov. Today 19 (2014) 1936–1944, https://doi.org/10.1016/j.drudis.2014.08.012.
[22] A. Kemble, B. Hornsperger, I. Ruf, H. Richter, B. Kuhn, M. Wittwer, B. Engelhardt, U. Grether, L. Collin, E. Development, R. Innovation, F.H. Roche, B. Sciences, A potent and selective inhibitor for the modulation of MAGL activity in the neurovasculature. https://doi.org/10.1101/2022.05.04.490688, 2022.
[23] M. Soethoudt, U. Grether, J. Fingerle, T.W. Grim, F. Fezza, L. de Petrocellis, C. Ullmer, B. Rothenhäusler, C. Perret, N. van Gils, D. Finlay, C. MacDonald, A. Chicca, M.D. Gens, J. Stuart, H. de Vries, N. Mastrangelo, L. Xia, G. Alachouzos, M.P. Baggelaar, A. Martella, E.D. Mock, H. Deng, L.H. Heitman, M. Connor, V. Di Marzo, J. Gertsch, A.H. Lichtman, M. Maccarrone, P. Pacher, M. Glass, M. van der Stelt, Cannabinoid CB2 receptor ligand profiling reveals biased signalling and off-target activity, Nat. Commun. 8 (2017), 13958, https://doi.org/10.1038/ncomms13958.
[24] A. Haider, J. Kretz, L. Gobbi, H. Ahmed, K. Atz, M. Bürkler, C. Bartelmus, J. Fingerle, W. Guba, C. Ullmer, M. Honer, I. Knuesel, M. Weber, A. Brink, A. M. Herde, C. Keller, R. Schibli, L. Mu, U. Grether, S.M. Ametamey, Structure-activity relationship studies of pyridine-based ligands and identification of a fluorinated derivative for positron emission tomography imaging of cannabinoid type 2 receptors, J. Med. Chem. 62 (2019) 11165–11181, https://doi.org/10.1021/acs.jmedchem.9b01280.